

Non-gaussianities and curvature perturbations from hybrid inflation

Sébastien Clesse,^{1,*} Björn Garbrecht,^{1,†} and Yi Zhu^{1,‡}

¹*Physik Department T70, James-Frank-Strasse, Technische Universität München, 85748 Garching, Germany*

(Dated: February 27, 2024)

For the original hybrid inflation as well as the supersymmetric F-term and D-term hybrid models, we calculate the level of non-gaussianities and the power spectrum of curvature perturbations generated during the waterfall, taking into account the contribution of entropic modes. We focus on the regime of mild waterfall, in which inflation continues for more than about 60 e-folds N during the waterfall. We find that the associated f_{NL} parameter goes typically from $f_{\text{NL}} \simeq -1/N_{\text{exit}}$ in the regime with $N \gg 60$, where N_{exit} is the number of e-folds between the time of Hubble exit of a pivot scale and the end of inflation, down to $f_{\text{NL}} \sim -0.3$ when $N \gtrsim 60$, i.e. much smaller in magnitude than the current bound from Planck. Considering only the adiabatic perturbations, the power spectrum is red, with a spectral index $n_s = 1 - 4/N_{\text{exit}}$ in the case $N \gg 60$, whereas in the case $N \gtrsim 60$ it increases up to unity. Including the contribution of entropic modes does not change observable predictions in the first case and the spectral index is too low for this regime to be viable. In the second case, entropic modes are a relevant source for the power spectrum of curvature perturbations, of which the amplitude increases by several orders of magnitudes. When spectral index values are consistent with observational constraints, the primordial spectrum amplitude is much larger than the observed value, and can even lead to black hole formation. We conclude that due to the important contribution of entropic modes, the parameter space leading to a mild waterfall phase is excluded by CMB observations for all the considered models.

PACS numbers: 98.80.Cq

I. INTRODUCTION

In the standard cosmological scenario, the large scale structures of the Universe are seeded by the quantum fluctuations of one or more scalar fields during a primordial phase of exponentially accelerated expansion. Due to this phase of inflation, the quantum field fluctuations becomes classical and are stretched outside the Hubble radius. They lead to a nearly scale invariant power spectrum of curvature perturbations \mathcal{P}_ζ , whose amplitude and spectral index are constrained by CMB observations. The recent results from the Planck experiment [1] give the best bounds with $\ln 10^{10} A_\zeta = 3.089 \pm 0.027$ and $n_s = 0.9603 \pm 0.0073$ with 68% C.L., where A_ζ is the value of $\mathcal{P}_\zeta(k_*)$ at the scale $k_* = 0.05 \text{Mpc}^{-1}$. Models of inflation predicting $n_s > 1$ are now ruled out at more than the 5σ level [2].

This is commonly thought to be the case of original hybrid inflation [3]. In this two-field model, inflation is realized in the false vacuum along a nearly flat valley of the field potential. It ends with a nearly instantaneous waterfall phase, triggered when the auxiliary field develops a tachyonic instability. Hybrid models are well motivated from the point of view of particle physics because they can be embedded in frameworks like supersymmetry [4–9], supergravity [10, 11] and Grand Unified Theories [12–14]. Other realizations of hybrid inflation in the

context of string theories [15–20], and extra-dimensional theories [21] have also been proposed.

In addition to a blue tilted power spectrum, the original hybrid model was thought to suffer from a problem of fine-tuning of initial field values [22, 23]. Moreover, because a Z_2 symmetry is broken at the end of inflation, it leads to the formation of domain walls with dramatic consequences for cosmology.

However, recent developments have shown that there exists a regime in the parameter space of the original hybrid model for which the final waterfall phase is sufficiently mild for inflation to continue for more than 60 e-folds N after the fields have crossed the critical instability point [24, 25]. In this scenario, topological defects are stretched outside the observable Universe, thus escaping observation, and the power spectrum of adiabatic perturbations is red, possibly in agreement with CMB observations. Moreover, the initial field values leading to inflation have been shown to occupy an important proportion of the field space in a large part of the potential parameter space [26–29], thus solving the fine-tuning problem of initial conditions. Similar conclusions have been obtained for the most well-known supersymmetric realizations of the hybrid model, the so-called F-term and D-term models [30]. In the standard regime of a fast waterfall, the contribution of the cosmic strings formed at the critical instability point must be considered for these models. The F-term model was nevertheless found to be in tension with WMAP data whereas the D-term model was strongly disfavoured [31, 32]. With the Planck results, the degeneracy between the spectral index and the string tension, that tends to favor larger values for the

* s.clesse@tum.de

† garbrecht@tum.de

‡ yi.zhu@tum.de

spectral index, is strongly reduced and both models appear to be ruled out in the standard regime [33].

The revival of the original hybrid scenario would be nevertheless of short duration if the mild waterfall scenario leads generically to a large level of non-gaussianities, with a local f_{NL} parameter outside the recent Planck bound $f_{\text{NL}} = 2.7 \pm 5.8$ (68% C.L.) [34], or if the power spectrum of curvature perturbations is strongly affected by the entropic modes along the waterfall trajectories.

The aim of this paper is to evaluate the power spectrum of curvature perturbations and the contribution of entropic modes, as well as the level of non-gaussianities produced in the mild waterfall regime, for the original hybrid scenario as well as for the supersymmetric F-term and D-term models. Our calculation therefore differs from Refs. [35–46] since they consider only the scenario of a waterfall phase lasting no more than a few e-folds. A similar calculation was performed in Ref. [47] for the original model, and some values for the parameters were found to lead to a large level of local f_{NL} , but the focus there was on super-planckian field evolution in a regime where the potential is dominated by the separable terms. A similar analysis is also performed in Ref. [48] but only for a single trajectory. In this paper, we use an unified parametrization of the potential for the three considered models (F-term, D-term and original hybrid inflation) and restrict the analysis to sub-planckian field values, such that supergravity corrections to the potential can be neglected. In this regime, the potential is not separable.

We use the δN formalism to calculate the local f_{NL} parameter, both analytically and numerically, as well as the amplitude and spectral index of the power spectrum of curvature perturbations. As a cross-check, we have also integrated numerically the linear multi-field perturbations and derived the exact power spectrum of curvature perturbations. This latter method has been chosen to study the time evolution of the field perturbations and their respective contribution to the adiabatic and entropic modes during the waterfall ¹.

Denoting by N_{exit} the number of e-folds between the time of Hubble exit of a pivot scale and the end of inflation, we find that the associated f_{NL} parameter goes typically from $f_{\text{NL}} \simeq -1/N_{\text{exit}}$, when the waterfall lasts for $N \gg 60$ e-folds, down to $f_{\text{NL}} \sim -0.3$ when $N \gtrsim 60$. In all cases the magnitude of f_{NL} does not exceed the bounds of Planck. Considering only the adiabatic perturbations, the power spectrum is red, with a spectral index $n_s = 1 - 4/N_{\text{exit}}$, in the case $N \gg 60$, whereas in the case $N \gtrsim 60$, it increases up to unity, which apparently suggests the presence of a parametric region, where the spectral index is in accordance with the observation

by Planck [25, 30]. When including the contribution of entropic modes, we find that the predictions do not change in the first case ($N \gg 60$). However, in the second case ($N \gtrsim 60$), entropic modes are a sizeable source for the power spectrum of curvature perturbations and the spectral index first takes lower values before eventually increasing up to unity. However, the amplitude of the power spectrum of curvature perturbations is enhanced by several orders of magnitudes and can even reach the level of black hole formation. We conclude that due to the important contribution of entropic modes, the parameter space leading to a mild waterfall phase is excluded by CMB observations for all the considered models.

This paper is organised as follows: in Sec. II we give the exact background multi-field dynamics. Then are introduced the δN formalism (Sec. III) and the linear theory of multi-field perturbations (Sec. IV). In Sec. V the considered hybrid models are briefly described and the unified parametrization of the potential is given. Sec. VI is dedicated to the slow-roll dynamics during the mild waterfall phase. In Secs. VII and VIII, we evaluate respectively the level of non-gaussianities and the power spectrum of curvature perturbations, and compare the analytical and numerical results. In the conclusion (Sec. IX), we discuss the impact of our results on the constraints of hybrid models and envisage interesting perspectives to this work.

II. MULTI-FIELD BACKGROUND DYNAMICS

Assuming that the Universe was filled with n nearly homogeneous real scalar fields $\phi_{i=1,2,\dots,n}$, the background dynamics is given by the Friedmann-Lemaître equations

$$H^2 = \frac{1}{3M_{\text{pl}}^2} \left[\frac{1}{2} \sum_{i=1}^n \dot{\phi}_i^2 + V(\phi_{i=1,\dots,n}) \right], \quad (1)$$

$$\frac{\ddot{a}}{a} = \frac{1}{3M_{\text{pl}}^2} \left[- \sum_{i=1}^n \dot{\phi}_i^2 + V(\phi_{i=1,\dots,n}) \right], \quad (2)$$

as well as by n coupled Klein-Gordon equations

$$\ddot{\phi}_i + 3H\dot{\phi}_i + \frac{\partial V}{\partial \phi_i} = 0, \quad (3)$$

where H is the Hubble expansion rate, $M_{\text{pl}} \equiv m_{\text{pl}}/\sqrt{8\pi}$ is the reduced Planck mass, $V(\phi_{i=1,\dots,n})$ is the field potential, and where a dot denotes the derivative with respect to the cosmic time t . Then one can define σ , the so-called *adiabatic field* [50], that describes the collective evolution of all the fields along the classical trajectory, and the velocity field

$$\dot{\sigma} \equiv \sqrt{\sum_{i=1}^n \dot{\phi}_i^2}. \quad (4)$$

¹ Notice that separable universe techniques can also be used to study the time evolution of both curvature and iso-curvature perturbations [49].

The equation of motion of the adiabatic field is given by

$$\ddot{\sigma} + 3H\dot{\sigma} + V_{\sigma} = 0, \quad (5)$$

where

$$V_{\sigma} \equiv \sum_{i=1}^n u_i \frac{\partial V}{\partial \phi_i}, \quad (6)$$

with u_i being the components of a unit vector along the field trajectory $u_i \equiv \dot{\phi}_i / \dot{\sigma}$.

III. THE δN FORMALISM

The δN formalism, based on the separate universe approximation (and other assumptions discussed e.g. in Ref. [51]), states that the curvature perturbation $\zeta(x, t)$ on a spatial hypersurface of uniform energy density is given by the difference between the number of e-folds realized from an initially flat hypersurface $N(t, x) \equiv \ln[\tilde{a}(t)/a(t_i)]$, where $\tilde{a}(t, x)$ is the local scale factor, and the unperturbed number of e-folds $N_0(t) \equiv \ln[a(t)/a(t_i)]$. If we label respectively by i and f the initial and final hypersurface, one has

$$\zeta = \delta N_i^f \equiv N(t, x) - N_0(t). \quad (7)$$

Our initial hypersurface is chosen at the time t_* corresponding to the Hubble exit of the observable pivot scale $k_* = 0.05 \text{ Mpc}^{-1}$ (in the rest of the paper, star subscripts indicate quantities evaluated at t_*). The final hypersurface must be of uniform energy density. In this paper we are interested in the curvature perturbations at the end of the slow-roll regime, when one of the slow-roll parameters reaches unity.

The field perturbations are close to Gaussian and have a very small amplitude, so that the observed curvature perturbations are given to good accuracy by

$$\zeta \simeq \sum_{i=1}^n N_{,i} \delta \phi_i + \frac{1}{2} \sum_{i,j=1}^n N_{,ij} \delta \phi_i \delta \phi_j, \quad (8)$$

where we have used the notation

$$N_{,i} \equiv \frac{\partial \delta N_i^f}{\partial \phi_i^i}, N_{,ij} \equiv \frac{\partial^2 \delta N_i^f}{\partial \phi_i^i \partial \phi_j^i}. \quad (9)$$

The amplitude of the reduced bispectrum is given by [52]

$$f_{\text{NL}} = -\frac{5}{6} \frac{\sum_{i,j} N_{,i} N_{,j} N_{,ij}}{(\sum_i N_{,i}^2)^2}. \quad (10)$$

One can also calculate the power spectrum amplitude and spectral tilt as

$$\mathcal{P}_{\zeta}(k_*) = \frac{H_*^2}{4\pi^2} \sum_i N_{,i}^2, \quad (11)$$

$$n_s - 1 = -2\epsilon_{1*} + \frac{2 \sum_{i,j} \dot{\phi}_i N_{,j} N_{,ij}}{H_* \sum_i N_{,i}^2}, \quad (12)$$

where $\epsilon_1 = -\dot{H}/H^2$ is the first slow-roll parameter. Practically, instead of a final surface of uniform density, we have chosen a final surface of constant field value, more precisely the value taken by the inflaton when the non-perturbed trajectory breaks the slow-roll approximation. As explained later in Section VII, the e-fold differences between these two surfaces is negligible compared to the e-folds variations between trajectories reaching them. This approximation leads therefore to accurate predictions. In addition, we have checked numerically for all the considered parameter sets that these two possible final surfaces give identical observable predictions.

We furthermore need to introduce the number of e-folds N^t in the sense of a reparameterization of time, $dN^t = H dt$, implying that during de Sitter inflation, where $a(t) = \exp(Ht)$, $N^t = Ht$. We use the subscript k to indicate its value when a given scale k exits the horizon, $*$ when this scale is the pivot scale and the subscript ‘end’ to indicate its value at a uniform density surface at the end of inflation. As stated above, the latter can be practically obtained by checking for the violation of the slow-roll conditions, cf. also the discussion in Section VII B. Finally we define the function

$$N \equiv N_{\text{end}}^t - N^t. \quad (13)$$

giving the number of e-folds up to the end of inflation.

IV. THE LINEAR THEORY OF MULTI-FIELD PERTURBATIONS

A. Perturbed equations

The perturbed metric can be written as

$$ds^2 = a^2 [-(1 + 2\Phi)d\eta^2 + (1 - 2\Psi)\delta_{ij}dx^i dx^j], \quad (14)$$

where Φ and Ψ are the Bardeen potentials and η is the conformal time, which is related to the cosmic time t as $dt = a d\eta$. In the longitudinal gauge, the spatial non-diagonal Einstein equations perturbed at first order lead to $\Phi = \Psi$, such that the $(0, 0)$, $(0, i)$ and (i, i) equations read

$$\begin{aligned} & -3\mathcal{H}(\Phi' + \mathcal{H}\Phi) + \nabla^2 \Phi \\ &= \frac{4\pi}{m_{\text{pl}}^2} \sum_{i=1}^n \left(\phi_i' \delta \phi_i' - \phi_i'^2 \Phi + a^2 \frac{\partial V}{\partial \phi_i} \delta \phi_i \right), \end{aligned} \quad (15)$$

$$\Phi' + \mathcal{H}\Phi = \frac{4\pi}{m_{\text{pl}}^2} \sum_{i=1}^n \phi_i' \delta \phi_i, \quad (16)$$

$$\begin{aligned} & \Phi'' + 3\mathcal{H}\Phi' + \Phi(2\mathcal{H}' + \mathcal{H}^2) \\ &= \frac{4\pi}{m_{\text{pl}}^2} \sum_{i=1}^n \left(\phi_i' \delta \phi_i' - \phi_i'^2 \Phi - a^2 \frac{\partial V}{\partial \phi_i} \delta \phi_i \right), \end{aligned} \quad (17)$$

where $\mathcal{H} \equiv a'/a$ and $\delta\phi_i$ is the perturbation of the scalar field ϕ_i , and where a prime denotes the derivative with respect to the conformal time. On the other hand, the n perturbed Klein-Gordon equations read

$$\delta\phi_i'' + 2\mathcal{H}\delta\phi_i' - \nabla^2\delta\phi_i + \sum_{j=1}^n a^2\delta\phi_j \frac{\partial^2 V}{\partial\phi_i\partial\phi_j} = 2(\phi_i'' + 2\mathcal{H}\phi_i')\Phi + 4\phi_i'\Phi'. \quad (18)$$

The field perturbations are coupled to each other through the cross derivatives of the potential and the Bardeen potential. By adding Eq. (15) to Eq. (17), and by using Eq. (16), one obtains the evolution equation for the Bardeen potential,

$$\Phi'' + 6\mathcal{H}\Phi' + (2\mathcal{H}' + 4\mathcal{H}^2)\Phi - \nabla^2\Phi = -\frac{8\pi}{m_{\text{pl}}^2}a^2 \sum_{i=1}^n \frac{\partial V}{\partial\phi_i} \delta\phi_i. \quad (19)$$

We want to obtain the curvature perturbation ζ , defined as

$$\zeta \equiv \Phi - \frac{\mathcal{H}}{\mathcal{H}' - \mathcal{H}^2}(\Phi' + \mathcal{H}\Phi). \quad (20)$$

The background dynamics implies that $\mathcal{H}' - \mathcal{H}^2 = -4\pi\sigma'^2/m_{\text{pl}}^2$. By using Eq. (16), the comoving curvature can thus be rewritten

$$\zeta = \Phi + \frac{\mathcal{H}}{\sigma'^2} \sum_{i=1}^n \phi_i' \delta\phi_i. \quad (21)$$

From the background and the perturbed Einstein equations, one can show that ζ evolves according to [53]

$$\zeta' = \frac{m_{\text{pl}}^2}{4\pi} \frac{\mathcal{H}}{\sigma'^2} \nabla^2\Phi - \frac{2\mathcal{H}}{\sigma'^2} \left[a^2 \sum_{i=1}^n \phi_i' \frac{\partial V}{\partial\phi_i} - \frac{a^2}{\sigma'^2} \left(\sum_{i=1}^n \phi_i' \frac{\partial V}{\partial\phi_i} \right) \left(\sum_{i=1}^n \phi_i' \delta\phi_i \right) \right] \quad (22)$$

$$= \frac{m_{\text{pl}}^2}{4\pi} \frac{\mathcal{H}}{\sigma'^2} \nabla^2\Phi - \frac{2\mathcal{H}}{\sigma'^2} \perp_{ij} a^2 \frac{\partial V}{\partial\phi_i} \delta\phi_j, \quad (23)$$

where the orthogonal projector $\perp_{ij} \equiv \text{Id} - u_i u_j$ has been introduced. For a single field model, the second term vanishes and one recovers the one-field evolution of ζ . For the multi-field case, one sees that entropy perturbations orthogonal to the field trajectory can be a source of curvature perturbations, even after Hubble exit.

B. Numerical integration

For the numerical integration of the perturbations, we refer to Ref. [53] and give here only the guidelines for the calculation of the exact power spectrum of curvature perturbations in a multi-field scenario. It is convenient to use the number of e-folds as the time variable. Some

equations are redundant, and one can for instance use the Bardeen potential expressed directly in terms of the field perturbations $\delta\phi_i$ and their derivatives. After expanding in Fourier modes, Eq. (18) reads [53]

$$\begin{aligned} & \frac{d^2\delta\phi_i}{dN^2} + (3 - \epsilon_1) \frac{d\delta\phi_i}{dN} \\ & + \sum_{j=1}^n \frac{1}{H^2} \frac{\partial^2 V}{\partial\phi_i\partial\phi_j} \delta\phi_j + \frac{k^2}{a^2 H^2} \delta\phi_i \\ & = 4 \frac{d\Phi}{dN} \frac{d\phi_i}{dN} - \frac{2\Phi}{H^2} \frac{\partial V}{\partial\phi_i}. \end{aligned} \quad (24)$$

Here, $\delta\phi_i = \delta\phi_i(k, \eta)$ and we may use $k = |\mathbf{k}|$ because of isotropy.

The quantization of the field perturbations in the limit $k \gg aH$ provides initial conditions for the $\delta\phi_i$. For the field operator, we take

$$\delta\phi_i(\eta, \mathbf{x}) = \int \frac{d^3k}{(2\pi)^3} \left[a_i(\mathbf{k}) e^{-i\mathbf{k}\cdot\mathbf{x}} \delta\phi_i(k, \eta) + \text{h.c.} \right], \quad (25)$$

where h.c. stands for hermitian conjugation and $[a_i(\mathbf{k}), a_j^\dagger(\mathbf{k}')] = (2\pi)^3 \delta_{ij} \delta(\mathbf{k} - \mathbf{k}')$. The normalized quantum modes are defined by

$$v_{i,k}(\eta) = a\delta\phi_i(k, \eta). \quad (26)$$

Neglecting the mass terms, they obey the equation $v_{i,k}'' + k^2 v_{i,k} = 0$, and in the regime $k \gg aH$, one has

$$\lim_{k/aH \rightarrow +\infty} v_{i,k}(\eta) = k e^{-ik(\eta - \eta_i)}. \quad (27)$$

In terms of the field perturbations, the initial conditions (denoted by the subscript i.c. to avoid confusion with previous notation) therefore read, up to a phase factor,

$$\delta\phi_{i,\text{i.c.}} = \frac{1}{\sqrt{2k}} \frac{1}{a_{\text{i.c.}}}, \quad (28)$$

$$\left[\frac{d\delta\phi_i}{dN^t} \right]_{\text{i.c.}} = -\frac{1}{a_{\text{i.c.}} \sqrt{2k}} \left(1 + i \frac{k}{a_{\text{i.c.}} H_{\text{i.c.}}} \right). \quad (29)$$

It is not convenient to integrate the perturbations from the onset of inflation, since the total number of e-folds can be much larger than N_* . In order to avoid the time consuming numerical integration of sub-Hubble modes behaving like plane waves, it is convenient to start to integrate the perturbations later, when the condition

$$\frac{k}{\mathcal{H}(n_{\text{i.c.}})} = C_k \gg 1 \quad (30)$$

is satisfied, where C_k is a constant characterizing the decoupling limit. To summarize, the numerical integration of multi-field perturbations can be divided in four steps:

1. The background dynamics is integrated until the end of inflation, such that N_{end}^t and $N_{\text{end}}^t - N_*^t$ are obtained.

2. The background dynamics is integrated again, until $N_{\text{i.c.}}^t$ is reached. Initial conditions for the perturbations are fixed at this time.
3. For each comoving mode k , the background and the perturbation dynamics are integrated simultaneously from $N_{\text{i.c.}}^t$ to N_{end}^t .
4. Determination of the scalar power spectrum, $\mathcal{P}_\zeta(k) = 1/(2\pi^2) \sum_i |\zeta_i|^2$, where $i = 1 \dots n$ stands for the n independent initial conditions for the field perturbations $\delta\phi_i$, ζ_i being the induced contributions to the curvature perturbation ζ .

V. HYBRID MODELS

A. Original version

The original hybrid model of inflation was first proposed by Linde [3]. Its potential reads

$$V(\phi, \psi) = \Lambda \left[\left(1 - \frac{\psi^2}{M^2} \right)^2 + \frac{\phi^2}{\mu^2} + \frac{2\phi^2\psi^2}{\phi_c^2 M^2} \right]. \quad (31)$$

The field ϕ is the inflaton, ψ is an auxiliary transverse field and M, μ, ϕ_c are three parameters of mass dimension. Inflation is assumed to be realized in the false vacuum [5] along the valley $\langle \psi \rangle = 0$. In the usual description, inflation ends when the transverse field develops a Higgs-type tachyonic instability soon after the inflaton reaches the critical value ϕ_c . From this point, the classical system is assumed to evolve quickly toward one of its true minima $\langle \phi \rangle = 0$, $\langle \psi \rangle = \pm M$, whereas in a realistic scenario one expects the instability to trigger a tachyonic preheating era [54–59].

B. Supersymmetric F-term model

Supersymmetric F -term inflation has been proposed in Refs. [4, 5] and has subsequently been discussed extensively in the literature. The underlying details for our present analysis are given in Ref. [30], and we only present the main assumptions and results for the potentials here. The superpotential is given by

$$W = \kappa \hat{S} (\hat{H} \hat{H} - m^2), \quad (32)$$

where the superfield \hat{S} is a gauge singlet and the superfields \hat{H} ($\hat{\bar{H}}$) transform in the (anti-)fundamental representation of $SU(\mathcal{N})$. This implies a tree-level scalar potential

$$V_0 = \kappa^2 (|\bar{H}H - m^2|^2 + |S\bar{H}|^2 + |SH|^2), \quad (33)$$

where now S , H and \bar{H} are complex scalar fields. The D -term gives a large mass to the field combination

$(1/\sqrt{2})(H - \bar{H})$, such that we do not need to consider this field direction for the dynamics of fluctuations during inflation. The waterfall field can be identified as $\psi = (1/\sqrt{2})(H + \bar{H})$ and the inflaton field as $\phi = \sqrt{2}|S|$. In terms of these degrees of freedom, the tree-level potential is

$$V_0(\phi, \psi) = \kappa^2 m^4 \left[\left(1 - \frac{\psi^2}{4m^2} \right)^2 + \frac{\phi^2 \psi^2}{4m^4} \right] \quad (34)$$

$$= \frac{\kappa^2}{4} \phi_c^4 \left[\left(1 - \frac{\psi^2}{2\phi_c^2} \right)^2 + \frac{\phi^2 \psi^2}{\phi_c^4} \right]. \quad (35)$$

In the potential valley where $\phi \geq \phi_c = \sqrt{2}m$ and $\langle \psi \rangle = 0$, the potential energy $\Lambda = \kappa^2 m^4$ spontaneously breaks supersymmetry. At one-loop order, this leads to the following correction to the potential:

$$V_1 = \frac{\kappa^4 \mathcal{N}}{128\pi^2} \left[(\phi^2 - \phi_c^2)^2 \log \left(\kappa^2 \frac{\phi^2 - \phi_c^2}{2Q^2} \right) + (\phi^2 + \phi_c^2)^2 \times \log \left(\kappa^2 \frac{\phi^2 + \phi_c^2}{2Q^2} \right) - 2\phi^4 \log \left(\frac{\kappa^2 \phi^2}{2Q^2} \right) \right], \quad (36)$$

where Q is a renormalization scale. Notice that the derivatives of this potential with respect to ϕ that are phenomenologically relevant for inflation are independent of Q .

We are concerned in this work with the dynamics near the critical point where $\phi \approx \phi_c$ and $\psi \approx 0$. As discussed in Ref. [30], treating the one-loop potential to linear order is a good approximation in that regime. Of relevance is the first derivative of the one-loop potential,

$$\left. \frac{\partial V_1(\phi)}{\partial \phi} \right|_{\phi=\phi_c} = \frac{\kappa^4 \mathcal{N}}{8\pi^2} \phi_c^3 \log 2. \quad (37)$$

In order to realize a substantial amount of e-folds below the critical point, the relation $\kappa \ll \phi_c^2/M_{\text{P}}^2$ must hold [30]. It can then easily be derived that the second derivatives of the one-loop potential may be neglected and that they do not yield a phenomenologically relevant contribution to the spectral tilt of the observable power spectrum [30].

C. Supersymmetric D-term model

Here, the superpotential is [6, 10]

$$W = \kappa \hat{S} \hat{H} \hat{\bar{H}}, \quad (38)$$

where \hat{S} is again a singlet and \hat{H} and $\hat{\bar{H}}$ transform according to the one-dimensional representation of a $U(1)$ gauge group. Spontaneous symmetry breaking is induced by the D -term

$$D = \frac{g}{2} (|H|^2 - |\bar{H}|^2 + m_{\text{FI}}^2), \quad (39)$$

where m_{FI} is the Fayet-Iliopoulos term. The inflaton field is again $\phi = \sqrt{2}|S|$, whereas now the waterfall field

is given by $\psi = \sqrt{2}|\bar{H}|$. The critical point, where ψ becomes tachyonically unstable is here

$$\phi_c = \frac{1}{\sqrt{2}} \frac{g}{\kappa} m_{\text{FI}}. \quad (40)$$

In terms of these various fields and variables, the tree-level potential can be expressed as

$$\begin{aligned} V_0 &= \kappa^2 (|H\bar{H}|^2 + |SH|^2 + |S\bar{H}|^2) + \frac{1}{2} D^2 \\ &= \frac{g^2}{8} m_{\text{FI}}^2 \left[\left(1 - \frac{\psi^2}{2m_{\text{FI}}^2} \right)^2 + 2 \frac{\kappa^2}{g^2} \frac{\phi^2 \psi^2}{m_{\text{FI}}^4} \right] \\ &= \frac{\kappa^4}{2g^2} \phi_c^4 \left[\left(1 - \frac{g^2}{4\kappa^2 \phi_c^2} \psi^2 \right)^2 + \frac{g^2}{2\kappa^2 \phi_c^4} \phi^2 \psi^2 \right]. \end{aligned} \quad (41)$$

The one-loop potential is readily obtained from its expression in the F -term case (36) when setting $\mathcal{N} = 1$.

D. Unified parametrization

In this paper, we study the original hybrid model as well as the supersymmetric F -term and D -term variants in a unified approach, by considering the following parametrization of the two-field potential,

$$V(\phi, \psi) = \Lambda \left[\left(1 - \frac{\psi^2}{M^2} \right)^2 + \left(\frac{\phi}{\mu} \right)^p + \frac{2\phi^2 \psi^2}{M^2 \phi_c^2} \right], \quad (42)$$

where M , ϕ_c are respectively the position of the global minima and of the critical point of instability along the valley. In the case of the original model, one has $p = 2$ whereas the dynamics for the F -term and D -term models near the instability point is well described when setting $p = 1$ [30]. The relations between the parameters of this potential and the model parameters for F -term and D -term inflation are given in TABLE I.

	F -term	D -term
Λ	$\kappa^2 m^4$	$\frac{\kappa^4}{2g^2} \phi_c^4 = \frac{g^2}{8} m_{\text{FI}}^4$
ϕ_c	$\sqrt{2}m$	$\frac{g}{\sqrt{2}\kappa} m_{\text{FI}}$
M	$2m$	$\sqrt{2}m_{\text{FI}}$
$1/\mu$	$\frac{\sqrt{2}\mathcal{N}\kappa^2 \log(2)}{4\pi^2 m}$	$\frac{\sqrt{2}\kappa g \log 2}{4\pi^2 m_{\text{FI}}}$

TABLE I. Parameters to be substituted into the potential (42) in order to obtain the F - and D -term models close to the critical point.

For the purpose of deriving the phenomenological consequences of hybrid inflation, it is useful to note the

derivatives

$$\frac{\partial V}{\partial \phi} = \frac{p\Lambda\phi^{p-1}}{\mu^p} \left(1 + \frac{4\mu^p\phi^{2-p}\psi^2}{pM^2\phi_c^2} \right), \quad (43a)$$

$$\frac{\partial V}{\partial \psi} = \frac{4\psi\Lambda}{M^2} \left(\frac{\phi^2 - \phi_c^2}{\phi_c^2} + \frac{\psi^2}{M^2} \right), \quad (43b)$$

$$\frac{\partial^2 V}{\partial \phi^2} = \frac{p(p-1)\Lambda\phi^{p-2}}{\mu^p} + \frac{4\Lambda\psi^2}{M^2\phi_c^2}, \quad (43c)$$

$$\frac{\partial^2 V}{\partial \psi^2} = \frac{4\Lambda}{M^2} \left(\frac{\phi^2 - \phi_c^2}{\phi_c^2} + \frac{3\psi^2}{M^2} \right), \quad (43d)$$

$$\frac{\partial^2 V}{\partial \phi \partial \psi} = \frac{8\Lambda\psi\phi}{M^2\phi_c^2}. \quad (43e)$$

In particular, the first derivatives enter the slow-roll equations of motion,

$$3H\dot{\phi} = -\frac{\partial V}{\partial \phi}, \quad 3H\dot{\psi} = -\frac{\partial V}{\partial \psi}, \quad H^2 = \frac{V}{3M_{\text{pl}}^2}. \quad (44)$$

We also make use of the standard definition for the slow-roll parameters $\eta_{XY} = M_{\text{pl}}^2 [\partial^2 V / (\partial X \partial Y)] / V$, where X and Y can be either of the canonically normalized fields ϕ and ψ .

VI. INFLATION ALONG WATERFALL TRAJECTORIES

We are interested in the field dynamics during the waterfall regime, i.e. in the times after the field trajectories cross the critical instability point ϕ_c . Tachyonic preheating is triggered when the exponentially growing long-wavelength perturbations of the auxiliary field ψ become non-linear. This only occurs when the tachyonic auxiliary field mass is larger than the Hubble expansion rate, $m_\psi^2 > H^2 \simeq V/(3M_{\text{pl}}^2)$, or equivalently when $-\eta_{\psi\psi} \gtrsim 1$. In the commonly studied large-coupling scenarios of hybrid inflation, this condition is satisfied after no more than a few e-folds after entering the waterfall phase. However, there exists a large region in the parameter space (the small coupling limit for the F -term and D -term models) for which the waterfall phase lasts for more than 60 e-folds. We refer to this situation as the mild waterfall. The field evolution in this regime has been studied for the original hybrid model in Refs. [24, 25], and for the F -term and D -term models in Ref. [30]. In this Section, we re-derive the mild waterfall dynamics for the unified potential of Eq. (42). For the purpose of an analytic description, we follow Ref. [25] and divide the field evolution below the critical point into three phases:

- Phase 0: when the second term of Eq. (43b) and the first term of Eq. (43a) dominate.
- Phase 1: when the first term of Eq. (43b) and the first term of Eq. (43a) dominate.
- Phase 2: when the first term of Eq. (43b) and the second term of Eq. (43a) dominate.

Classically, the phase 0 does not last more than about one e-fold [25]. Moreover, in a realistic scenario, the quantum diffusion of the auxiliary field dominates over the classical dynamics very close to the critical instability point. For these reasons we do not consider the phase 0 but only the phases 1 and 2.

Following the derivation of Ref. [25], it is convenient to parameterize the fields as

$$\phi \equiv \phi_c e^\xi, \quad \psi \equiv \psi_0 e^\chi, \quad (45)$$

where ψ_0 is the initial condition for the auxiliary field at the critical point of instability. During the slow-roll waterfall regime, one has $\xi < 0$ and $|\chi| \ll 1$, which is consistently verified by the explicit solutions.

A. Phase 1

Solving the slow-roll equations, one finds that the field trajectories during the phase 1 follow the relation

$$\xi^2 = \frac{pM^2\phi_c^{p-2}}{4\mu^p}(\chi - \chi_i) \quad (46)$$

as long as the temporal minimum (corresponding to the ellipse where $dV/d\psi$ vanishes) is not reached. In this case, phase 1 connects to phase 2 at the point (ξ_2, χ_2) , with

$$\chi_2 \equiv \ln \left(\frac{\sqrt{p}\phi_c^{\frac{p}{2}}M}{2\mu^{p/2}\psi_0} \right). \quad (47)$$

One obtains the number of e-folds realized in phase 1 by integrating

$$\frac{d\xi}{dN^t} \simeq -\frac{p\phi_c^{p-2}M_{\text{pl}}^2}{\mu^p}. \quad (48)$$

Imposing that $N^t = 0$ at the critical point, one finds

$$\xi = -\frac{pM_{\text{pl}}^2\phi_c^{p-2}}{\mu^p}N^t. \quad (49)$$

The temporal minimum for the field ψ is located on the trajectories

$$\xi = -\frac{\psi_0^2 e^{2\chi}}{2M^2}. \quad (50)$$

It is reached during phase 1 if the condition

$$\chi_2 < \frac{p\phi_c^{p+2}}{16\mu^p M^2} \quad (51)$$

is satisfied. One therefore gets

$$\xi_2 \equiv \begin{cases} -\frac{\sqrt{p}\phi_c^{\frac{p}{2}-1}M}{2\mu^{p/2}}\sqrt{\chi_2} & \text{for } \chi_2 > \frac{p\phi_c^{p+2}}{16\mu^p M^2} \\ -\frac{p\phi_c^p}{8\mu^p} & \text{for } \chi_2 < \frac{p\phi_c^{p+2}}{16\mu^p M^2} \end{cases}. \quad (52)$$

The number of e-folds N_1 realized in phase 1 then follows as

$$N_1 = \begin{cases} \frac{\sqrt{\chi_2}\mu^{p/2}M}{2\sqrt{p}\phi_c^{\frac{p}{2}-1}M_{\text{pl}}^2} & \text{for } \chi_2 > \frac{p\phi_c^{p+2}}{16\mu^p M^2} \\ \frac{\phi_c^2}{8M_{\text{pl}}^2} & \text{for } \chi_2 < \frac{p\phi_c^{p+2}}{16\mu^p M^2} \end{cases}. \quad (53)$$

B. Phase 2

The slow-roll equations in phase 2 yield the trajectory

$$\xi^2 = \xi_2^2 + \frac{pM^2\phi_c^{p-2}}{8\mu^p} \left[e^{2(\chi - \chi_2)} - 1 \right]. \quad (54)$$

Once again, we have to distinguish between the possibility where this trajectory reaches the temporal minimum at some point before the end of inflation, and the possibility where the temporal minimum is not reached during inflation. In phase 2, the temporal minimum is reached when

$$\xi = \xi_{2\text{T.M.}} \equiv -\frac{M^2}{2\phi_c^2} - \sqrt{\frac{M^4}{4\phi_c^4} + \xi_2^2 - \frac{p\phi_c^p}{8\mu^p}}. \quad (55)$$

On the other hand, inflation ends before reaching the temporal minimum when

$$\eta_{\psi\psi} \simeq \frac{8M_{\text{pl}}^2\xi}{M^2} \simeq -1. \quad (56)$$

In the opposite case, where the temporal minimum is reached before the end of inflation, the slow-roll conditions are violated when

$$\eta_{\phi\phi} \simeq \frac{4M_{\text{pl}}^2\psi^2}{\phi_c^2 M^2} \simeq 1. \quad (57)$$

By using Eq. (50), one thus finds that

$$\xi_{\text{end}} = \begin{cases} -\frac{\phi_c^2}{8M_{\text{pl}}^2} & \text{for } |\xi_{\text{end}}| > |\xi_{2\text{T.M.}}| \\ -\frac{M^2}{8M_{\text{pl}}^2} & \text{for } |\xi_{\text{end}}| < |\xi_{2\text{T.M.}}| \end{cases}. \quad (58)$$

During phase 2 and before reaching the temporal minimum, assuming that $\xi \ll 1$ and $\chi_2 > 1/2$, the slow-roll equations in e-fold time can be solved exactly and one finds [25]

$$\xi(N^t) = c' \sqrt{\frac{pM^2}{2\phi_c^{p-2}\mu^p}} \frac{(c' - c)f(N^t) - c' - c}{(c' - c)f(N^t) + c' + c}, \quad (59)$$

where $c \equiv \sqrt{\chi_2/2}$, $c' \equiv \sqrt{c^2 - 1/4}$ and

$$f(N^t) = \exp \left[\frac{8\sqrt{2}c'p\phi_c^{\frac{p}{2}-1}M_{\text{pl}}^2(N^t - N_1)}{\sqrt{p\mu^p M^2}} \right]. \quad (60)$$

A good approximation can be obtained by considering the limit $|\xi| \gg |\xi_2|$, where one can obtain

$$\frac{1}{\xi} - \frac{1}{\xi_{\text{end}}} = \frac{8M_{\text{pl}}^2}{M^2}(N^t - N_{\text{end}}^t). \quad (61)$$

The number of e-folds realised along the temporal minimum is obtained by integrating

$$\frac{d\xi}{dN^t} = \frac{8M_{\text{pl}}^2\xi}{\phi_c^2}. \quad (62)$$

This gives

$$N_{\text{end}}^t - N_{2\text{T.M.}}^t = \frac{\phi_c^2}{8M_{\text{pl}}^2} \ln\left(\frac{\xi_{\text{end}}}{\xi_{2\text{T.M.}}}\right), \quad (63)$$

where $N_{2\text{T.M.}}^t$ is the value of the parameter N^t when $\xi = \xi_{2\text{T.M.}}$. If we understand the model specified by the potential (42) as an effective theory valid below the Planck scale, we should impose that $\phi_c \ll M_{\text{pl}}$ and consequently, the number of e-folds inflation continues for after reaching the temporal minimum is very low.

VII. NON GAUSSIANTITIES FROM THE MILD WATERFALL PHASE

A. Analytical results

In this Section, we calculate the level of non-gaussianities using the δN formalism. We denote the time where the transition between the phases 1 and 2 occurs by $t_{1,2}$ and the time of Hubble exit of the pivot scale k_* by t_* . We need to distinguish the case when the pivot scale leaves the Hubble radius in phase 2 (case 1: long waterfall phase with $N_{\text{end}}^t \gg 60$, and $t_* > t_{1,2}$) from the case where horizon exit occurs in phase 1 (case 2: moderately long waterfall phase, with $N_{\text{end}}^t \gtrsim 60$ and $t_* < t_{1,2}$).

1. Case 1: Hubble exit in phase 2

The first step for calculating the local f_{NL} parameter with the δN formalism is to derive the number of e-folds until the end of inflation starting from an arbitrary initial point (ξ_i, χ_i) in field space. In order to compare with the observational bounds, we then use this result to evaluate the quantities $N_{,\phi}$, $N_{,\psi}$, $N_{,\phi\phi}$, $N_{,\phi\psi}$ and $N_{,\psi\psi}$ for the pivot scale k_* , at which the unperturbed background fields take the values (ξ_*, χ_*) .

We first consider the case where inflation ends before the temporal minimum is reached. Integrating the slow-roll equation of motion in phase 2 give the trajectories

$$\psi^2 = \psi_0^2 e^{2\chi} = 2\phi_c^2(\xi^2 - \xi_i^2) + \psi_0^2 e^{2\chi_i}. \quad (64)$$

(This equation also determines χ_{end} when replacing $\xi \rightarrow \xi_{\text{end}}$ and $\chi \rightarrow \chi_{\text{end}}$.) Above relation can be used in combination with the slow-roll equation for ϕ to derive the number of e-folds that elapse while the fields evolve from (ξ_i, χ_i) to $(\xi_{\text{end}}, \chi_{\text{end}})$,

$$N_{\text{end}}^t - N_i^t = -\frac{M^2}{8M_{\text{pl}}^2} \int_{\xi_i}^{\xi_{\text{end}}} \frac{d\xi}{\xi^2 - \xi_i^2 + \frac{\psi_0^2 e^{2\chi_i}}{2\phi_c^2}}. \quad (65)$$

Defining $C \equiv -\xi_i^2 + \psi_0^2 e^{2\chi_i} / (2\phi_c^2)$, one finds

$$N_{\text{end}}^t - N_i^t = -\frac{M^2}{8M_{\text{pl}}^2 \sqrt{C}} \times \left[\arctan\left(\frac{\xi_{\text{end}}}{\sqrt{C}}\right) - \arctan\left(\frac{\xi_i}{\sqrt{C}}\right) \right] \quad (66)$$

if $C > 0$, and

$$N_{\text{end}}^t - N_i^t = -\frac{M^2}{8M_{\text{pl}}^2 \sqrt{C}} \times \left[\operatorname{arctanh}\left(\frac{\xi_{\text{end}}}{\sqrt{C}}\right) - \operatorname{arctanh}\left(\frac{\xi_i}{\sqrt{C}}\right) \right] \quad (67)$$

if $C < 0$.

For applying the δN formalism, we need to evaluate the e-fold derivatives with respect to ϕ_i and ψ_i , evaluated in the limit where $\xi_i \rightarrow \xi$ and $\chi_i \rightarrow \chi$, where ξ and χ belong to the unperturbed waterfall trajectory, and for which the relations

$$\psi_0^2 e^{2\chi} = 2\phi_c^2 \xi^2 \quad (68)$$

and

$$\xi = -\frac{M^2}{8M_{\text{pl}}^2 \left(N_{\text{end}}^t - N^t - \frac{M^2}{8M_{\text{pl}}^2 \xi_{\text{end}}} \right)}. \quad (69)$$

are satisfied. Note that in this limit, one gets $C \rightarrow 0$ and one can expand Eqs. (66) and (67) in a Taylor series to obtain

$$N_{\text{end}}^t - N_i^t = \frac{M^2}{8M_{\text{pl}}^2} \left(\frac{1}{\xi_{\text{end}}} - \frac{1}{\xi_i} + \frac{|C|}{3\xi_i^3} - \frac{|C|}{3\xi_{\text{end}}^3} \right), \quad (70)$$

which is a consistent generalization of Eq. (61). We use this expression to calculate the e-fold derivatives $N_{,\phi}$, $N_{,\psi}$, $N_{,\phi\phi}$, $N_{,\phi\psi}$ and $N_{,\psi\psi}$ around the field configuration (ξ_i, χ_i) . For the purpose of calculating these derivatives, we can now relabel $(\xi_i, \chi_i) \rightarrow (\xi, \chi)$. [I.e. ξ has now a different purpose than the integration variable in Eq. (65)]. We thus obtain

$$N_{,\phi} = \frac{M^2}{8\phi_c e^\xi M_{\text{pl}}^2} \left(\frac{1}{\xi^2} - \frac{2}{3\xi^2} + \frac{2\xi}{3\xi_{\text{end}}^3} \right) \simeq \frac{M^2}{24\phi_c M_{\text{pl}}^2 \xi^2} \quad (71)$$

and

$$N_{,\psi} = \frac{M^2}{8M_{\text{pl}}^2} \left(\frac{\psi}{3\phi_c^2 \xi^3} - \frac{\psi}{3\phi_c^2 \xi_{\text{end}}^3} \right) \simeq \frac{M^2 \psi}{24\phi_c^2 M_{\text{pl}}^2 \xi^3}. \quad (72)$$

The approximations above are valid when $|\xi| < |\xi_{\text{end}}|$ and thus $|\xi^3| \ll |\xi_{\text{end}}^3|$. As we eventually replace $\xi \rightarrow \xi_*$, these relations are well satisfied for the present purposes. By using $\psi = -\sqrt{2}\phi_c \xi$, we notice the useful relation

$$N_{,\phi} = -\frac{1}{\sqrt{2}} N_{,\psi}. \quad (73)$$

For the second derivatives, when keeping only the leading terms, we find

$$N_{,\psi\psi} = \frac{M^2}{24\phi_c^2 M_{\text{pl}}^2} \left(\frac{1}{\xi^3} - \frac{1}{\xi_{\text{end}}^3} \right) \simeq \frac{M^2}{24\phi_c^2 M_{\text{pl}}^2 \xi^3}, \quad (74)$$

$$N_{,\phi\phi} \simeq \frac{4M^2}{24\phi_c^2 M_{\text{pl}}^2 \xi^3} \quad (75)$$

and

$$N_{,\phi\psi} = -\frac{M^2 \psi_k}{8\phi_c^3 e^\xi M_{\text{pl}}^2 \xi^3} \simeq \frac{3\sqrt{2}M^2}{24M_{\text{pl}}^2 \phi_c^2 \xi^3}. \quad (76)$$

One can now evaluate the f_{NL} parameter at the pivot scale k_* . We first notice that

$$N_{,\phi\phi} = 4N_{,\psi\psi} \simeq \frac{4}{3\sqrt{2}} N_{,\phi\psi}. \quad (77)$$

Using that the number of e-folds inflation lasts after the horizon exit of the pivot scale is given by $N_{\text{exit}} = N_{\text{end}}^t - N_*^t$ and evaluating above derivatives for $(\xi, \chi) = (\xi_*, \chi_*)$, we obtain

$$f_{\text{NL}} \simeq \frac{5}{18} \left(\frac{24M_{\text{pl}}^2 \xi_*}{M^2} \right) \simeq -\frac{5}{3(N_{\text{exit}} - \frac{M^2}{8M_{\text{pl}}^2 \xi_{\text{end}}})} \ll 1. \quad (78)$$

In the case of the F-term and D-term models, this expression reduces to

$$f_{\text{NL}} \simeq -\frac{5}{3(N_{\text{exit}} + 1)}. \quad (79)$$

The level of non-gaussianities is therefore negative and very low, typically $f_{\text{NL}} \approx -0.03$ for the F-term and D-term models.

We finally consider the situation where the temporal minimum for the field ψ is reached in phase 2 before the end of inflation. Then, we need to evaluate

$$N = N_*^{\text{T.M.}} + N_{\text{T.M.}}^{\text{end}}. \quad (80)$$

The first term on the right hand side is the number of e-folds realised between t_* and the time where the temporal

minimum is reached. The second term is the number of e-folds realised along the temporal minimum up to the end of inflation.

Starting from an arbitrary initial field value in phase 2, one finds the value of ξ at which the trajectory crosses the temporal minimum,

$$\xi_{2\text{T.M.}} = -\frac{M^2}{2\phi_c^2} - \sqrt{\frac{M^4}{4\phi_c^4} + \xi_i^2 + \psi_i^2/(2\phi_c^2)} \quad (81)$$

For evaluating $N_{*,\phi}^{\text{T.M.}}$, one can take Eq. (70) and replace ξ_{end} by $\xi_{2\text{T.M.}}$. For the derivatives, we again replace $(\xi_i, \chi_i) \rightarrow (\xi, \chi)$ and notice that

$$\frac{d\xi_{2\text{T.M.}}}{d\xi} = \frac{-\xi}{\frac{M^2}{2\phi_c^2} - \xi_{2\text{T.M.}}}. \quad (82)$$

This gives an additional term $-(d\xi_{2\text{T.M.}}/d\phi_i)/\xi_{\text{T.M.}}^2$ in the round brackets of Eq. (71), that is negligible compared to the leading term. Next, using Eq. (63), one can calculate

$$N_{\text{T.M.,}\phi}^{\text{end}} = \frac{\phi_c}{8M_{\text{pl}}^2 \xi_{2\text{T.M.}}} \frac{d\xi_{2\text{T.M.}}}{d\xi} = \frac{\phi_c}{M_{\text{pl}}^2} \mathcal{O}(\xi). \quad (83)$$

Since $|\xi| < |\xi_{\text{end}}| = \phi_c^2/(8M_{\text{pl}}^2)$, we find that $N_{\text{T.M.,}\phi}^{\text{end}} \ll N_{*,\phi}^{\text{T.M.}}$, provided $\phi_c \ll M_{\text{pl}}$, as one should require for the effective theory description to be valid.

In a similar way, one finds that the leading terms in $N_{\text{T.M.,}\psi}^{\text{end}}$, $N_{\text{T.M.,}\psi\psi}^{\text{end}}$, $N_{\text{T.M.,}\phi\psi}^{\text{end}}$ and $N_{\text{T.M.,}\phi,\phi}^{\text{end}}$, as well as in f_{NL} , are not modified when the temporal minimum is reached, apart that one has to replace ξ_{end} by $\xi_{\text{T.M.}}$. As a consequence, the level of non-gaussianities is reduced compared to the contributions from $N_*^{\text{T.M.}}$ and cannot in any case increase up to an observable level.

2. Case 2: Hubble exit in phase 1

Now we consider the situation where the pivot scale exits the Hubble radius in the phase 1. We first consider the case where the temporal minimum is not reached. In order to obtain the spectra using the δN approach, we need to generalize the analysis of Section VI A, where we have fixed the initial value of ξ to zero, to more general initial values ξ_i , such that we can obtain the necessary e-fold derivatives.

By integrating the slow-roll equations of motion, we obtain the trajectory

$$\xi^2 - \xi_i^2 = \frac{p\phi_c^{p-2} M^2 (\chi - \chi_i)}{4\mu^p}. \quad (84)$$

Eq. (48) gives the number of e-folds elapsing from the point (ξ_i, χ_i) until reaching (ξ_{2i}, χ_2) , where phase 1 ends,

$$N_1 = N_2^t - N_i^t = -\frac{\mu^p (\xi_{2i} - \xi_i)}{pM_{\text{pl}}^2 \phi_c^{p-2}}, \quad (85)$$

where $\xi_{2i} = -\sqrt{\xi_i^2 + p\phi_c^{p-2}M^2(\chi_2 - \chi_i)/(4\mu^p)}$, N_i^t is the value of the parameter N^t at the initial point (ξ_i, χ_i) , N_2^t its value at (ξ_{2i}, χ_2) , and χ_2 is again given by Eq. (47).

The number of e-folds between the point (ξ_i, χ_i) and the point where inflation ends in phase 2 due to the violation of the slow-roll conditions is then given by $N_1 + N_2$, where N_2 are the e-folds between the onset of phase 2 (ξ_{2i}, χ_2) and the violation of slow roll. For the following purposes, we can again drop the index i on the initial field values, i.e. $(\xi_i, \chi_i) \rightarrow (\xi, \chi)$ and $(\phi_i, \psi_i) \rightarrow (\phi, \psi)$. The e-fold first derivatives then read

$$N_{,\phi} = \frac{1}{\phi_k} (N_{1,\xi} + N_{2,\xi}) , \quad (86)$$

$$N_{,\psi} = \frac{1}{\psi_k} (N_{1,\chi} + N_{2,\chi}) . \quad (87)$$

We first evaluate Eq. (87). The first term gives

$$N_{1,\chi} = -\frac{\mu^p}{p\phi_c^{p-2}M_{\text{pl}}^2} \frac{d\xi_{2i}}{d\chi} = \frac{M^2}{8M_{\text{pl}}^2\xi_2} , \quad (88)$$

and the second term yields

$$N_{2,\chi} = -\frac{p\phi_c^{p-2}M^2}{16\xi_2\mu^p} \frac{dN_2}{d\xi_{2i}} . \quad (89)$$

Using Eq. (70) with ξ_{2i} and χ_{2i} instead of ξ_i and χ_i for the number of e-folds realized in phase 2, one gets

$$\frac{dN_2}{d\xi_{2i}} = \frac{M^2}{8M_{\text{pl}}^2\xi_{2i}^2} \left(1 - \frac{2}{3} + \frac{2\xi_{2i}^3}{3\xi_{\text{end}}^3}\right) \simeq \frac{M^2}{24M_{\text{pl}}^2\xi_{2i}^2} , \quad (90)$$

and thus one obtains

$$N_{2,\chi} = -\frac{p\phi_c^{p-2}M^4}{384\xi_2^3M_{\text{pl}}^2\mu^p} = -\frac{1}{12\chi_2}N_{1,\chi} , \quad (91)$$

where the last expression is found by inserting the value of ξ_2 from Eq. (52). Since $\chi_2 > \mathcal{O}(1)$ [it is a large logarithm *cf.* Eq. (47)], the dominant term in Eq. (87) comes from the number of e-folds realised during phase 1. In the following, we will therefore neglect the term $N_{2,\chi}$, such that

$$N_{,\psi} \simeq \frac{M^2}{8M_{\text{pl}}^2\xi_2\psi} . \quad (92)$$

We now turn to Eq. (86). For the first term, one finds

$$\frac{dN_1}{d\xi} = -\frac{\mu^p}{pM_{\text{pl}}^2\phi_c^{p-2}} \left(\frac{\xi}{\xi_2} - 1\right) \quad (93)$$

and for the second term,

$$\frac{dN_2}{d\xi} = \frac{dN_2}{d\xi_{2i}} \frac{\xi}{\xi_2} \approx \frac{M^2\xi}{24M_{\text{pl}}^2\xi_2^3} . \quad (94)$$

Using the appropriate expression from Eq. (52) for ξ_2^2 , one sees that

$$\frac{dN_1}{d\xi} = 6\chi_2 \left(\frac{\xi_2}{\xi} - 1\right) \frac{dN_2}{d\xi} . \quad (95)$$

Hence again, we may neglect the contribution coming from the number of e-folds in phase 2 and obtain from Eq. (93)

$$N_{,\phi} \simeq \frac{\mu^p}{pM_{\text{pl}}^2\phi_c^{p-1}} . \quad (96)$$

Moreover, since $\psi_* \ll \psi_2$, we may use that $N_{,\phi} \ll N_{,\psi}$.

For the second derivatives, one can again show that the dominant terms come from the number of e-folds in phase 1. One therefore obtains

$$\begin{aligned} N_{,\psi\psi} &= -\frac{M^2}{8M_{\text{pl}}^2\xi_2\psi^2} \left(1 + \frac{1}{2\chi_2}\right) \\ &\simeq -\frac{M^2}{8M_{\text{pl}}^2\xi_2\psi^2} \simeq -\frac{1}{\psi} N_{,\psi} , \end{aligned} \quad (97)$$

$$N_{,\phi\psi} \simeq -\frac{M^2\xi}{8M_{\text{pl}}^2\xi_2^3\phi_c\psi} \simeq -\frac{\xi}{\xi_2^2\phi_c} N_{,\psi} , \quad (98)$$

and

$$N_{,\phi\phi} = \frac{\mu^p}{pM_{\text{pl}}^2\phi_c^{p-2}\phi^2} \left(-1 + \frac{\xi}{\xi_2} - \frac{1}{\xi_2} + \frac{\xi^2}{\xi_2^3}\right) \quad (99)$$

$$\simeq -\frac{\mu^p}{pM_{\text{pl}}^2\phi_c^{p-2}\xi_2\phi_c^2} . \quad (100)$$

Now we can evaluate the parameter f_{NL} in the limit where the derivatives with respect to the field ϕ as well as the contribution from the number of efolds in phase 2 are negligible. One finds

$$\begin{aligned} f_{\text{NL}} &\simeq -\frac{5}{6} \frac{N_{,\psi\psi}(N_{,\psi})^2}{(N_{,\psi})^4} \simeq \frac{20M_{\text{pl}}^2\xi_2}{3M^2} \\ &\simeq -\frac{10\sqrt{p}M_{\text{pl}}^2\phi_c^{p/2-1}}{3M\mu^{p/2}} \sqrt{\chi_2} . \end{aligned} \quad (101)$$

For the F-term model, this implies

$$|f_{\text{NL}}| \simeq \frac{5\kappa\sqrt{\mathcal{N}}\sqrt{\log 2}M_{\text{pl}}^2}{6\sqrt{2}\pi m^2} \sqrt{\chi_2} \lesssim 0.13\sqrt{\chi_2} \quad (102)$$

where the maximal negative value of f_{NL} is obtained when the waterfall lasts just about 60 e-folds, i.e. when $\kappa\sqrt{\mathcal{N}} \approx m^2/M_{\text{pl}}^2$ [30]. Particle physics experiments impose a lower bound on m , inducing the upper bound $\sqrt{\chi_2} \lesssim 6$. The negative amplitude of the f_{NL} parameter is therefore never higher than about unity, which is below the Planck sensitivity. We have plotted in FIG. 1 the level of local non-gaussianities given by Eqs. (101) and (78), as a function of κ for the F-term model with different values of m . For the D-term model, the level of

non-gaussianities is given by the same expression, with m_{FI} instead of m . It is independent of the model parameter g , apart logarithmically through the $\sqrt{\chi_2}$ factor.

For the original model, requiring 60 e-folds along the waterfall imposes $M\mu \gtrsim 40M_{\text{pl}}^2$ [24]. The level of non-gaussianities is independent of the parameters Λ and ϕ_c (apart through $\sqrt{\chi_2}$), and its maximal negative value is therefore of about $f_{\text{NL}} \simeq -0.3$, as for the F-term and D-term models. In TABLE II we give the level of non-gaussianities from the analytical approximations in the original model for various parameter sets, covering the qualitatively different regimes, and compare to the numerical results. Notice finally that the particular case where the temporal minimum is reached in phase 1 is not relevant, because that would imply that $\chi_2 \ll 1$ and thus the quantum diffusion would still be dominating at the time of Hubble exit of the observable scales.

At this point, we can justify our choice of a final hypersurface fixed at $\xi = \xi_{\text{end}}$, instead of a surface of constant energy density. Considering only the phase-2, one gets that ψ_{end} is given by

$$\psi_{\text{end}}^2 = 2\phi_c^2 (\xi_{\text{end}}^2 - \xi_i^2) + \psi_i^2 \quad (103)$$

In the context of the δN formalism, one can evaluate the shift $\Delta(\psi_{\text{end}}^2)$ induced by a perturbations of the fields at the time of Hubble crossing of the pivot scale. For a perturbation of the auxiliary field, one gets

$$\frac{\Delta(\psi_{\text{end}}^2)}{\Delta\psi_*} = 2\psi_* = 2\sqrt{2}\phi_c\xi_* \quad (104)$$

whereas a perturbation of the ϕ field leads to

$$\frac{\Delta(\psi_{\text{end}}^2)}{\Delta\phi_*} = 4\phi_c\xi_* \quad (105)$$

The potential at the end of inflation is given by

$$V(\phi_{\text{end}}, \psi_{\text{end}}) = \Lambda \left(1 + 2\xi_{\text{end}} \frac{\psi_{\text{end}}^2}{M^2} \right) \quad (106)$$

and therefore, in order to reach a surface of constant density, the shift in ψ_{end} should be compensated by a shift in ξ_{end} , which reads respectively

$$\frac{\Delta\xi_{\text{end}}}{\Delta\psi_*} = \frac{4\sqrt{2}\phi_c\xi_*}{M^2}, \quad (107)$$

$$\frac{\Delta\xi_{\text{end}}}{\Delta\phi_*} = \frac{8\phi_c\xi_*}{M^2}. \quad (108)$$

Considering that $\xi_* \simeq -M^2/(8M_{\text{pl}}^2 N_*)$, one obtains that

$$\frac{\Delta\xi_{\text{end}}}{\Delta\psi_*} = \frac{\sqrt{2}}{2} \frac{\Delta\xi_{\text{end}}}{\Delta\phi_*} \ll 1. \quad (109)$$

In the limit $|\xi_*| \gg |\xi_{\text{end}}|$, the corresponding shift in Eqs. (71), (72), (75), (74) and (76) induced by the different

choices for the final hypersurface can therefore be safely neglected.

In the case where the pivot scale exits the Hubble radius in phase-1 one can evaluate the shift of ξ_2^2 as $\Delta\xi_2^2 = -\Delta\xi_*^2$ and $\Delta\xi_2^2 = -p\phi_c^{p-2}M^2\Delta\chi_*/(4\mu^p)$ for field perturbations respectively in the longitudinal and transverse directions. By using $\Delta(\psi_{\text{end}}^2) = -2\phi_c^2\Delta\xi_2^2$ and then $\Delta\xi_{\text{end}} = 2\Delta\psi_{\text{end}}^2/M^2$, it is straightforward to show that

$$\frac{\Delta\xi_{\text{end}}}{\Delta\psi_*} \ll 1, \quad \frac{\Delta\xi_{\text{end}}}{\Delta\phi_*} \ll 1. \quad (110)$$

Since the dominant terms in $N_{,\phi}$, $N_{,\psi}$, $N_{,\phi\phi}$, $N_{,\psi\psi}$ and $N_{,\phi\psi}$ come from the variation of the number of e-folds in phase 1, and because here again the shift in the terms coming from the number of e-folds in phase 2 can be neglected, one can conclude that our results are independent of the possible choices for the final hypersurface.

B. Numerical analysis

The analytical results of the previous Section are valid under some approximations, namely: i) the slow-roll approximation, ii) a sharp transition between phase 1 and phase 2, iii) the final hypersurface given by the condition $\xi = \xi_{\text{end}}$ [according to Eq. (58)] instead of a uniform density condition, iv) the Taylor expansion (70) of the number of e-folds in phase 2, v) some terms neglected in the e-folds derivatives. To check the validity and the accuracy of our results, we have implemented a numerical calculation that makes use of the δN formalism. Practically, we use the following algorithm:

1. First, a numerical integration of the exact multi-field background dynamics, from the critical instability point, where we set $N^t = 0$, until the end of inflation in order to obtain the total number of e-folds N_{end}^t of inflation along that part of the field trajectory.
2. Second, an integration of the background dynamics from the critical point down to the time t_* of Hubble exit of the pivot scale $k_* = 0.05\text{Mpc}^{-1}$. With the help of the first step, we know that the exit point is reached when the e-fold parameter equals $N_*^t = N_{\text{end}}^t - N_{\text{exit}}$.
3. Numerical integration of the field dynamics from initial conditions on a 3×3 grid of values centered on (ϕ_*, ψ_*) . Determination of the number of e-folds N to reach the final hypersurface.
4. Numerical evaluation of the derivatives $N_{,i}$ and $N_{,ij}$. The f_{NL} parameter as well as the amplitude \mathcal{P}_ζ and the spectral tilt n_s of the power spectrum of curvature perturbations can then be computed by using Eqs. (10), (11) and (12).

For the stability of the code, notice that the differences between the initial conditions need to be carefully chosen,

sufficiently small for the numerical derivatives $N_{,i}$ and $N_{,ij}$ to be accurate, but at the same time sufficiently large for the differences between the values of N to be much larger than the integration steps (that cannot be lower than $\Delta N \sim 10^{-4}$ without increasing unreasonably the integration computing time).

Another numerical issue is related to the choice of the final hypersurface. It is particularly tricky to define it numerically because the variation of the false vacuum potential along the waterfall trajectories is so tiny that it cannot be resolved due to the limited numerical precision. We have thus considered the following alternatives: i) by defining the final hypersurface as the end of the slow-roll regime, more precisely when one of the slow-roll parameters reaches unity, ii) by implementing the uniform energy condition after the end of inflation, when for instance $\rho_{\text{end}} = 0.99\rho_{\text{inf}}$ (in this case the effects of the tachyonic preheating are considered to be negligible and the classical trajectories are assumed to be valid down to the final hypersurface), iii) by defining a hypersurface of uniform potential energy density without including the constant term $V_0 = \Lambda$. We did not find noticeable differences between these possible methods.

At the critical instability point, the classical dynamics of the auxiliary field is dominated by the quantum diffusion. Classical trajectories must therefore be seen as emerging from this quantum stochastic regime. They are valid once the classical vacuum expectation value of the auxiliary field fulfills $\psi \gg \sqrt{\langle \psi_{\text{qu}}^2 \rangle}$, where ψ_{qu} is the operator for the quantum field fluctuations around the classical expectation value ψ . For the numerical integration of the field dynamics, we take for the initial condition of the auxiliary field at the critical instability point the value given by the process of quantum diffusion [24, 30]

$$\psi_0 \simeq \frac{\sqrt{\kappa} M_{\text{F}}^3}{2\sqrt{3}\pi^{3/4}(\ln 2)^{1/4}} \quad \text{for the F-term,} \quad (111)$$

$$\psi_0 \simeq \frac{gm_{\text{FI}}^3}{8\sqrt{3}\pi^{3/4}(\ln 2)^{1/4}} \quad \text{for the D-term,} \quad (112)$$

$$\psi_0 \simeq \sqrt{\frac{\Lambda\mu M}{96\pi^{3/2}}} \quad \text{for the original model} \quad (113)$$

and only consider the trajectory as valid when $\psi \gg \psi_0$.

For the F-term model, we have plotted in Fig. 1 the local f_{NL} parameter calculated numerically as a function κ , for different values of the mass parameter m in the range $10^{-4}M_{\text{pl}} < M < 0.1M_{\text{pl}}$. For comparison, the analytical approximations derived in the previous Section are also presented. Numerical and analytical results agree well, with f_{NL} values ranging typically from -0.03 down to -0.3 , as long as $m \lesssim 0.01M_{\text{pl}}$. For larger values, in the regime $t_* < t_{1,2}$, our approximation given by Eq. (101) is not valid any more and the $|f_{\text{NL}}|$ parameter takes lower values. This is because the e-folds derivatives with respect to the field ϕ become an important contribution to the level of non-gaussianities. We can draw identical conclusions for the D-term model, where the level of non-gaussianity is nearly independent of the coupling g .

For the original model, the parameter space has two additional dimensions and it is more difficult to explore it entirely with our numerical method. However, we present in TABLE II a comparison of numerical and analytical results for a few sets of parameters corresponding to the different regimes. This serves as a check that the numerical results are in agreement with the analytical approximations.

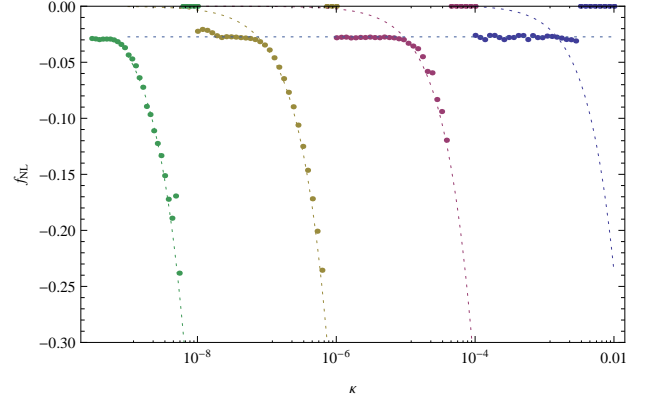


FIG. 1. Local f_{NL} parameter as a function of κ , for the F-term model, with from left to right $m = 10^{-4}M_{\text{pl}}$, $m = 10^{-3}M_{\text{pl}}$, $m = 10^{-2}M_{\text{pl}}$, $m = 10^{-1}M_{\text{pl}}$. The bold dots are the numerical results using the δN formalism. The dotted horizontal line corresponds to $f_{\text{NL}} = -5/[3(N_{\text{exit}} + 1)]$ [the approximate result from Eq. (101)] and the dashed lines to Eq. (101), which are respectively valid for $t_* > t_{1,2}$ and $t_* < t_{1,2}$. We assume for simplicity that $N_{\text{exit}} = 60$.

VIII. POWER SPECTRUM OF CURVATURE PERTURBATIONS AND CONTRIBUTION OF ENTROPIC MODES

A. Using the δN formalism

The amplitude and spectral index of the power spectrum of curvature perturbations at the end of inflation can be calculated by using the δN formalism, as explained in Section III. For the spectral index, in addition to the e-folds derivatives that have been calculated in the previous Section, one needs to know the field derivatives at the time of Hubble exit of the pivot scale.

1. Case 1: Hubble exit in phase 2

In the generic case where $t_* > t_{1,2}$, one obtains

$$\frac{d\phi}{dN^t} = -\frac{8M_{\text{pl}}^2\phi_c\xi^2}{M^2} = -\frac{1}{3N_{,\phi}}, \quad (114)$$

$$\frac{d\psi}{dN^t} = \sqrt{2}\frac{8M_{\text{pl}}^2\phi_c\xi^2}{M^2} = -\frac{1}{3N_{,\psi}}. \quad (115)$$

Parameters	Regime	$f_{\text{NL}}^{\text{num}}$	$f_{\text{NL}}^{\text{app}}$	n_s^{num}	n_s^{app}	$\mathcal{P}_\zeta^{\text{num}}(k_*)$	$\mathcal{P}_\zeta^{\text{app}}(k_*)$
$M = \phi_c = 0.01 M_{\text{pl}}, \mu = 10^5 M_{\text{pl}}, \Lambda = 10^{-20} M_{\text{pl}}^4$	$t_{1,2} < t_*$	-0.030	-0.029	0.929	0.930	0.017	0.019
$M = \phi_c = 0.001 M_{\text{pl}}, \mu = 10^6 M_{\text{pl}}, \Lambda = 10^{-30} M_{\text{pl}}^4$	$t_{1,2} < t_*$	-0.033	-0.033	0.921	0.921	1.1×10^{-6}	1.3×10^{-6}
$M = 0.001 M_{\text{pl}}, \phi_c = 10^{-5}, \mu = 10^6 M_{\text{pl}}, \Lambda = 10^{-30} M_{\text{pl}}^4$	$t_{1,2} < t_*$	-0.033	-0.032	0.921	0.921	0.0011	0.012
$M = 0.01 M_{\text{pl}}, \phi_c = 0.1 M_{\text{pl}}, \mu = 10^5 M_{\text{pl}}, \Lambda = 10^{-20} M_{\text{pl}}^4$	$t_{1,2} < t_* < t_{TM}$	-0.030	-0.030	0.929	0.929	1.8×10^{-4}	1.9×10^{-4}
$M = 0.001 M_{\text{pl}}, \phi_c = 0.1 M_{\text{pl}}, \mu = 10^6 M_{\text{pl}}, \Lambda = 10^{-30} M_{\text{pl}}^4$	$t_{1,2} < t_* < t_{TM}$	-0.033	-0.032	0.921	0.921	1.1×10^{-10}	1.3×10^{-10}
$M = \phi_c = 0.01 M_{\text{pl}}, \mu = 10^4 M_{\text{pl}}, \Lambda = 10^{-20} M_{\text{pl}}^4$	$t_* < t_{1,2}$	-0.10	-0.11	0.881	0.880	0.23	0.29
$M = \phi_c = 0.01 M_{\text{pl}}, \mu = 10^{3.8} M_{\text{pl}}, \Lambda = 10^{-20} M_{\text{pl}}^4$	$t_* < t_{1,2}$	-0.17	-0.18	0.946	0.955	1.2	1.36
$M = \phi_c = 0.001 M_{\text{pl}}, \mu = 10^5 M_{\text{pl}}, \Lambda = 10^{-30} M_{\text{pl}}^4$	$t_* < t_{1,2}$	-0.14	-0.15	0.78	0.77	2.9×10^{-4}	4.6×10^{-4}
$M = \phi_c = 0.001 M_{\text{pl}}, \mu = 10^{4.8} M_{\text{pl}}, \Lambda = 10^{-30} M_{\text{pl}}^4$	$t_* < t_{1,2}$	-0.23	-0.24	0.77	0.77	0.021	0.035
$M = 0.001 M_{\text{pl}}, \phi_c = 10^{-4} M_{\text{pl}}, \mu = 10^5 M_{\text{pl}}, \Lambda = 10^{-30} M_{\text{pl}}^4$	$t_* < t_{1,2}$	-0.12	-0.13	0.82	0.81	6.1×10^{-3}	8.4×10^{-3}
$M = 0.001 M_{\text{pl}}, \phi_c = 10^{-4} M_{\text{pl}}, \mu = 10^{4.8} M_{\text{pl}}, \Lambda = 10^{-30} M_{\text{pl}}^4$	$t_* < t_{1,2}$	-0.20	-0.21	0.83	0.84	0.15	0.21

TABLE II. Comparison of the power spectrum, its tilt and the non-gaussianities in the original model for various illustrative points in parameter space, representing the horizon exit of the pivot scale during the qualitatively different phases. We compare the approximate analytical results with the numerical results obtained using the δN formalism, assuming instantaneous reheating.

Because observable scales exit the Hubble radius near the critical instability point, one has $\epsilon_* \ll 1$, so that it can be neglected. Using Eq. (12), one then finds

$$n_s - 1 \simeq \frac{32\xi_* M_{\text{pl}}^2}{M^2} \simeq -\frac{4}{\left(N_{\text{exit}} - \frac{M^2}{8M_{\text{pl}}^2\xi_{\text{end}}}\right)}. \quad (116)$$

This formula corresponds to the one derived in Refs. [25, 30] assuming that the waterfall trajectories are effectively single-field. For the amplitude of the power spectrum of curvature perturbations, one gets

$$\begin{aligned} \mathcal{P}_\zeta(k_*) &\simeq \frac{\Lambda M^4}{16 \times 24^2 \pi^2 M_{\text{pl}}^6 \phi_c^2 \xi_*^4} \\ &\simeq \frac{4\Lambda M_{\text{pl}}^2 \left(N_{\text{exit}} - \frac{M^2}{8M_{\text{pl}}^2\xi_{\text{end}}}\right)^4}{9\pi^2 M^2 \phi_c^2} \end{aligned} \quad (117)$$

Here also the results of Refs. [25, 30] are recovered. Therefore the regime corresponding to $t_* > t_{1,2}$ is effectively single field. The F-term and D-term models generate a red tilted power spectrum, but the spectral index is too low when compared to CMB observations. For the original model, it is in principle possible to increase its value up to $n_s \simeq 0.94$ by increasing Λ that is a free parameter, and therefore N_{exit} . However, in this case inflation is realised at an energy scale near the limit imposed by the search for B -mode polarization in the CMB.

Finally, for the original model, notice that our comment regarding the specific case where the trajectories reach the temporal minimum before the end of inflation still applies, and ξ_{end} can be replaced by $\xi_{2,\text{TM}}$ in Eq. (117).

2. Case 2: Hubble exit in phase 1

In the case where the potential parameters are tuned such that $t_* < t_{1,2}$, we find

$$\frac{d\phi}{dN^t} = -\frac{p\phi_c^{p-1}M_{\text{pl}}^2}{\mu^p} = -\frac{1}{N_{,\phi}}, \quad (118)$$

$$\frac{d\psi}{dN^t} = -\frac{8M_{\text{pl}}^2\psi\xi}{M^2} = -\frac{\xi}{N_{,\psi\xi_2}}. \quad (119)$$

By using these equations as well as the relations $N_{,\psi} \gg N_{,\phi}$, $N_{,\psi\psi} \gg N_{,\psi\phi}$ and $N_{,\psi\psi} \gg N_{,\phi\phi}$, we obtain the leading term for the spectral index

$$n_s - 1 \simeq \frac{16M_{\text{pl}}^2\xi_*}{M^2}. \quad (120)$$

When $\xi_* \rightarrow \xi_2$ it is connected to the spectral index for $t_* > t_{1,2}$. Notice that instead of increasing when the Hubble exit occurs deeper in phase 1, the spectral index first takes lower values than expected for effectively single-field trajectories. This behaviour is shown in FIG. 5 that gives the spectral index as a function of κ for the F-term model and different values of M . This is because $|\xi_2|$, and thus $|\xi_*|$, first increases with κ . The spectral index increases up to unity only when $\xi_* \rightarrow 0$. From Eq. (120) only, one can conclude that it is possible to find a spectral index value in agreement with CMB observations. It turns out however, that the power spectrum amplitude is strongly modified in this case by entropy perturbations and cannot fit to CMB observations, as explained in the following.

The amplitude of the power spectrum is given by

$$\mathcal{P}_\zeta(k_*) \simeq \frac{\Lambda M^2 \mu^p}{192\pi^2 p M_{\text{pl}}^6 \phi_c^{p-2} \chi_2 \psi_*^2}. \quad (121)$$

In the case where $t_* \simeq t_{1,2}$, we replace $\psi_* = \psi_0 \exp(\chi_2)$,

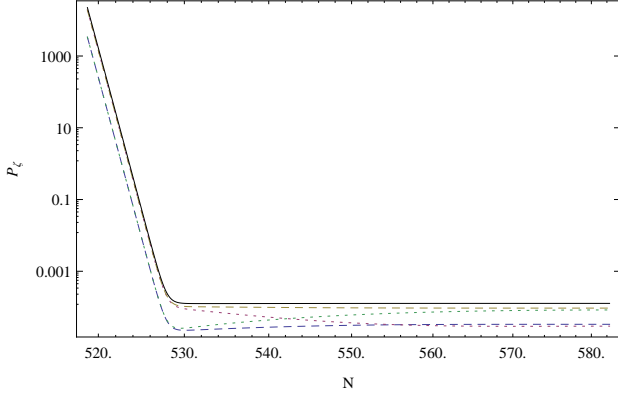


FIG. 2. Evolution of the power spectrum of curvature perturbations (black) as well as of rescaled adiabatic (dashed) and entropic (dotted) perturbations, generated respectively by initial perturbations of ϕ (blue and red curves) and ψ (green and yellow curves), and the power spectrum of curvature perturbations (black curve) for a pivot scale $k_* = 0.05 \text{Mpc}^{-1}$ and F-term potential parameters $m = 10^{-3}$ and $\kappa = 5 \times 10^{-8}$. These parameters correspond to the case $t_* > t_{1,2}$.

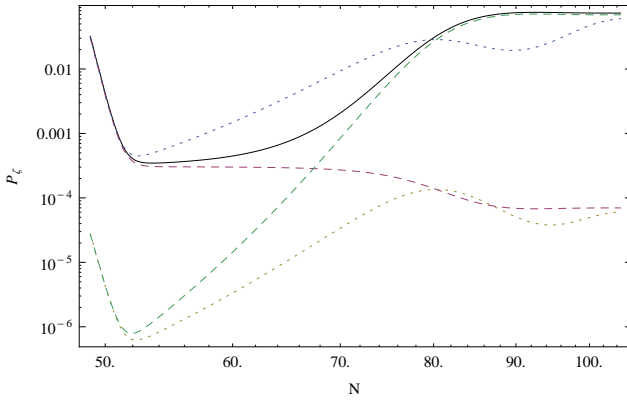


FIG. 3. Evolution of the power spectrum of curvature perturbations (black) as well as of rescaled adiabatic (dashed) and entropic (dotted) perturbations, sourced respectively by initial perturbations of ϕ (blue and red curves) and ψ (green and yellow curves), and the power spectrum of curvature perturbations (black curve) for a pivot scale $k_* = 0.05 \text{Mpc}^{-1}$ and F-term potential parameters $m = 10^{-3}$ and $\kappa = 3 \times 10^{-7}$. These parameters correspond to the case $t_* < t_{1,2}$.

such that the amplitude is

$$\mathcal{P}_\zeta(k_*, t_* \simeq t_{1,2}) \simeq \frac{\Lambda \mu^{2p}}{48\pi^2 p^2 M_{\text{pl}}^6 \phi_c^{2p-2} \chi_2}, \quad (122)$$

and it connects continuously to what is found in Eq. (117) for $t_* > t_{1,2}$. When the Hubble exit of the scale k_* occurs deeper in phase 1, we see using Eqs. (46) and (49) that

the amplitude grows exponentially as

$$\mathcal{P}_\zeta(k_*) \times \exp \left[2\chi_2 \left(1 - \frac{N_*^{t^2}}{N_1^2} \right) \right], \quad (123)$$

where N_1 is the number of e-folds in phase 1 (between the critical point and the transition to phase 2) and N_t^* is the number of e-folds between the critical point and the horizon exit of the scale k_* (i.e. the value of the parameter N^t at horizon exit, provided $N^t = 0$ at the critical point). The spectrum then may reach a maximal amplitude typically larger than unity,

$$\mathcal{P}_\zeta(t_* \simeq 0) \simeq \frac{\Lambda M^2 \mu^p}{192\pi^2 p^2 M_{\text{pl}}^6 \phi_c^{p-2} \chi_2 \psi_0^2}. \quad (124)$$

It is important to notice that there is no freedom to fix the amplitude of the curvature power spectrum independently of its spectral index, because ψ_* in Eq. 121 is related to ξ_* through Eq. 46 describing the waterfall trajectory in phase-1. Then, considering that ψ_0 takes values given by Eqs. (111), (112) or (113) depending on the model and that χ_2 only depends logarithmically on the model parameters (it is typically of order unity and cannot be used to rescale by a significant amount the amplitude of the spectrum), one can see that for parameter values $\kappa \sim M^2/M_{\text{pl}}^2$ or $M\mu \sim M_{\text{pl}}^2$ (to which corresponds the regime where $N_{\text{end}} \gtrsim 60$ and Hubble exit of observable modes in phase-1), the power spectrum amplitude is several order of magnitudes larger than 10^{-9} .

FIGs. 4 and 5 for the F-term model illustrate this exponential growth that prevents the amplitude to be in agreement with CMB observations when the spectral tilt is in the allowed range by CMB observations. As mentioned in the previous Section, the case where the temporal minimum is reached in phase 1 is not relevant because of the quantum diffusion.

B. From the numerical integration of multi-field perturbations

We now compare with the results obtained from the methods explained in Section IV. By integrating the multi-field perturbations, one can follow their sub-Hubble and super-Hubble evolution throughout the waterfall phase and identify the contributions of the fields to the rescaled adiabatic and entropic perturbations, that are respectively defined as [53]

$$\delta\pi_a = \frac{\dot{\phi}\delta\phi}{\sqrt{\dot{\phi}^2 + \dot{\psi}^2}} + \frac{\dot{\psi}\delta\psi}{\sqrt{\dot{\phi}^2 + \dot{\psi}^2}}, \quad (125)$$

$$\delta\pi_e = \frac{\dot{\psi}\delta\phi}{\sqrt{\dot{\phi}^2 + \dot{\psi}^2}} + \frac{\dot{\phi}\delta\psi}{\sqrt{\dot{\phi}^2 + \dot{\psi}^2}}. \quad (126)$$

We have plotted on FIGs. 2 and 3 the evolution of curvature, rescaled adiabatic and entropic perturbations for

the F-term model (but we find similar behaviors for the D-term and the original models) for the case $t_* > t_{1,2}$ and $t_* < t_{1,2}$, respectively.

In the first case, the curvature perturbations freeze when they become super-Hubble, as expected for an effectively single field model. Notice also that in the sub-Hubble regime, the adiabatic perturbations induced by the initial conditions for $\delta\phi$ with $\delta\psi$ initially set to zero correspond to the entropy perturbations induced by $\delta\psi$ with $\delta\phi$ initially set to zero, and conversely. This is expected because the field perturbations evolve as independent plane waves with identical amplitudes in the sub-Hubble regime, and because

$$\delta\pi_a = \cos\theta\delta\phi - \sin\theta\delta\psi, \quad (127)$$

$$\delta\pi_e = \sin\theta\delta\phi + \cos\theta\delta\psi, \quad (128)$$

where θ is the angle between a unit vector tangential to the field trajectory and the $\phi = 0$ direction.

In the second case ($t_* < t_{1,2}$), we observe that super-Hubble curvature perturbations receive contributions from entropy perturbations that are generated during the field evolution in phase 1 and then are frozen during the phase 2. This corresponds to the strong enhancement of the power spectrum amplitude according to Eq. (123) obtained within the δN formalism.

We have compared the analytical approximations of the previous Section to the numerical results for the power spectrum amplitude and spectral index. For the F-term model, we have plotted in Figs. 4 and 5 the amplitude and the spectral index of the power spectrum of curvature perturbations as a function of the parameter κ , for various values of M in the F-term model. For comparison, we have also plotted the effective 1-field slow-roll predictions and the analytical approximations derived in the previous Section. These plots illustrate the general agreement we find between the different methods, and the important modification of the power spectrum of curvature perturbations when compared to the predictions assuming an effectively single-field dynamics. As expected, for the D-term model we find very similar results.

For the original model, we have compared in TABLE II the power spectrum amplitude and spectral index for some parameter sets corresponding to the different regimes. For the spectrum amplitude, we observe a strong discrepancy (up to 30%) between numerical results and the analytical approximation in the regime where $t_* < t_{1,2}$. However, it must be noticed that a tiny modification of $N_2^t - N_{\text{end}}^t$ can affect importantly the spectrum amplitude in this regime. Since this quantity cannot be evaluated analytically with a very good precision (even more since we assume a sharp transition between phase 1 and phase 2, which is not exactly the case), such a strong discrepancy can be explained. In the case $t_* > t_{1,2}$, numerical and analytical results agree well. Finally, we observe that when the temporal minimum is reached in phase 2 before the end of inflation, the predictions from the numerical and the approximate analytical method only show marginal deviations, because

$|\xi_{2,\text{TM}}| \approx M^2/\phi_c^2 \ll 1$ in this parametric regime.

IX. CONCLUSION

Using two different methods – the δN formalism and the numerical integration of the linear multi-field perturbations – we have calculated the level of non-gaussianities and the power spectrum of curvature perturbations produced in the parametric regime of a mild waterfall phase in models of hybrid inflation.

We have investigated the supersymmetric F-term and D-term models as well as the original non-supersymmetric hybrid model. In order to study these within a unified analysis, we have introduced a common parametrisation for the different variants of the potential. For the F-term and D-term models, the mild waterfall regime occurs in the small coupling limit, when $\kappa \lesssim M^2/M_{\text{pl}}^2$. For the original model this happens when $\mu M > M_{\text{pl}}^2$. We have only considered field values lower than Planck mass, as it is commonly imposed for an effective field theory description to be valid. The defining feature of the mild waterfall regime is that the last 60 e-folds of inflation are realized after the fields pass the critical point, such that possible cosmological defects are stretched outside the observable Universe. The observational predictions are modified, and if one assumes that the waterfall trajectories are effectively single-field, one obtains spectral index values from $n_s = 1 - 4/N_{\text{exit}}$, when observable scales leave the Hubble radius in the so-called slow-roll phase 2 where the slope of the potential in the valley direction is dominated by the terms involving the auxiliary field of the waterfall ($t_* > t_{1,2}$), and up to unity when this happens in the first phase ($t_* < t_{1,2}$), where the slope along the inflationary valley dominates. Prior to the present analysis, the model was therefore considered as possibly in agreement with CMB observations [25, 30]. However, since the scalar field trajectories are turning during the waterfall regime toward the minima of the potential, one might expect a large contribution of entropic modes to the power spectrum of curvature perturbations, as well as a high level of local non-gaussianities. The quantification of these contributions and the resulting signatures and the resolution of the question of the phenomenological viability of hybrid inflation in the mild waterfall regime are the main results of the present paper. For this purpose, we have derived analytical approximations for the local f_{NL} parameter and the power spectrum amplitude and tilt, which agree well with the numerical results.

For all the models, we find that the generic regime corresponding to $t_* > t_{1,2}$ is effectively described by single field dynamics, with $f_{\text{NL}} \approx -5/(3(N_{\text{exit}} + 1)) \approx 0.03$, which is nearly independent of the potential parameters. For the spectrum amplitude and the spectral index, we confirm the results of Refs. [24, 25, 30] by using both the δN formalism and the linear theory of multi-field perturbations. The resulting spectral index is outside and

below the bounds imposed by CMB experiments, and this regime is therefore strongly disfavored.

For the particular regime where the parameters are tuned so that $t_* < t_{1,2}$, we find that the waterfall trajectories cannot be considered as effectively single field. The level of non-gaussianities increases, with negative values of f_{NL} down to about minus unity. Notice however that in no case we find that the level of non-gaussianity exceeds the recent bounds from the Planck experiments. Regarding the power spectrum of curvature perturbations, we find that the entropic modes are an important source of the super-Hubble curvature perturbations, enhancing the power spectrum by several order of magnitudes, up to a maximal amplitude larger than unity, which is far from the CMB constraints and which would lead to the formation of primordial black holes. When scales exit the Hubble radius deeper in the first slow-roll phase, the spectral index first takes lower values than expected for an effectively single field model, and then increases up to unity. However, values for the spectral index that are in agreement with CMB constraints always appear in conjunction with a power spectrum amplitude that is much higher than the measured one. Contrary to what was thought before [24, 25, 30], it is therefore impossible to find parameters in agreement with CMB observations.

We leave for a future work the particular case where the waterfall lasts typically $1 < N \lesssim 60$, for which we expect a modification of the slow-roll prediction of infla-

tion along the valley. We also would like to emphasize that the levels of non-gaussianities are calculated in this paper at the end of the inflationary era. In principle, they can be subsequently modified during the reheating era. In Ref. [60], some models are found for which the non-gaussianities are enhanced during the reheating. But in the context of a tachyonic preheating phase, applying the δN formalism seems to be a very challenging issue. Another interesting perspective would be to forecast the constraints on hybrid models from the CMB distortions generated by the perturbations from the waterfall phase at the end of inflation. Finally, we would like to mention that in the regime where the dynamics of both the fields is stochastic [61], observable predictions have not been derived so far. Studying this regime will nevertheless require new methods since the classical dynamics is not valid in this case.

ACKNOWLEDGEMENTS

The authors acknowledge support by the DFG cluster of excellence ‘Origin and Structure of the Universe’. In addition, SC has received funding from the Alexander von Humboldt Foundation, BG from the Gottfried Wilhelm Leibniz programme of the DFG and YZ from the Chinese Scholarship council. The authors warmly thank Christophe Ringeval for useful comments and discussion.

-
- [1] P. Ade *et al.* (Planck Collaboration), (2013), arXiv:1303.5076 [astro-ph.CO].
 - [2] P. Ade *et al.* (Planck Collaboration), (2013), arXiv:1303.5082 [astro-ph.CO].
 - [3] A. D. Linde, Phys. Rev. **D49**, 748 (1994), arXiv:astro-ph/9307002.
 - [4] G. R. Dvali, Q. Shafi, and R. K. Schaefer, Phys. Rev. Lett. **73**, 1886 (1994), arXiv:hep-ph/9406319.
 - [5] E. J. Copeland, A. R. Liddle, D. H. Lyth, E. D. Stewart, and D. Wands, Phys. Rev. **D49**, 6410 (1994), arXiv:astro-ph/9401011.
 - [6] P. Binétruy and G. R. Dvali, Phys. Lett. **B388**, 241 (1996), arXiv:hep-ph/9606342.
 - [7] R. Kallosh and A. Linde, JCAP **0310**, 008 (2003), arXiv:hep-th/0306058.
 - [8] B. Clauwens and R. Jeannerot, JCAP **0803**, 016 (2008), arXiv:0709.2112 [hep-ph].
 - [9] B. Garbrecht, C. Pallis, and A. Pilaftsis, JHEP **12**, 038 (2006), arXiv:hep-ph/0605264.
 - [10] E. Halyo, Phys. Lett. **B387**, 43 (1996), arXiv:hep-ph/9606423.
 - [11] P. Binétruy, G. Dvali, R. Kallosh, and A. Van Proeyen, Class. Quant. Grav. **21**, 3137 (2004), arXiv:hep-th/0402046.
 - [12] R. Jeannerot, Phys. Rev. **D56**, 6205 (1997), arXiv:hep-ph/9706391.
 - [13] R. Jeannerot, S. Khalil, G. Lazarides, and Q. Shafi, JHEP **10**, 012 (2000), hep-ph/0002151.
 - [14] T. Fukuyama, N. Okada, and T. Osaka, JCAP **0809**, 024 (2008), arXiv:0806.4626 [hep-ph].
 - [15] F. Koyama, Y. Tachikawa, and T. Watari, Phys. Rev. **D69**, 106001 (2004), arXiv:hep-th/0311191.
 - [16] G. R. Dvali and S. H. H. Tye, Phys. Lett. **B450**, 72 (1999), arXiv:hep-ph/9812483.
 - [17] M. Berkooz, M. Dine, and T. Volansky, Phys. Rev. **D71**, 103502 (2005), arXiv:hep-ph/0409226.
 - [18] S. C. Davis and M. Postma, JCAP **0804**, 022 (2008), arXiv:0801.2116 [hep-th].
 - [19] P. Brax *et al.*, JCAP **0701**, 026 (2007), arXiv:hep-th/0610195.
 - [20] S. Kachru *et al.*, JCAP **0310**, 013 (2003), arXiv:hep-th/0308055.
 - [21] M. Fairbairn, L. Lopez Honorez, and M. H. G. Tytgat, Phys. Rev. **D67**, 101302 (2003), hep-ph/0302160.
 - [22] L. E. Mendes and A. R. Liddle, Phys. Rev. **D62**, 103511 (2000), arXiv:astro-ph/0006020.
 - [23] N. Tetradis, Phys. Rev. **D57**, 5997 (1998), arXiv:astro-ph/9707214.
 - [24] S. Clesse, Phys. Rev. **D83**, 063518 (2011), arXiv:1006.4522 [gr-qc].
 - [25] H. Kodama, K. Kohri, and K. Nakayama, Prog. Theor. Phys. **126**, 331 (2011), arXiv:1102.5612 [astro-ph.CO].
 - [26] S. Clesse, C. Ringeval, and J. Rocher, Phys. Rev. **D80**, 123534 (2009), arXiv:0909.0402 [astro-ph.CO].

- [27] S. Clesse and J. Rocher, Phys. Rev. **D79**, 103507 (2009), arXiv:0809.4355 [hep-ph].
- [28] S. Clesse, AIP Conf. Proc. **1241**, 543 (2010), arXiv:0910.3819 [astro-ph.CO].
- [29] R. Easther and L. C. Price, (2013), arXiv:1304.4244 [astro-ph.CO].
- [30] S. Clesse and B. Garbrecht, Phys.Rev. **D86**, 023525 (2012), arXiv:1204.3540 [hep-ph].
- [31] R. Battye, B. Garbrecht, and A. Moss, Phys. Rev. **D81**, 123512 (2010), arXiv:1001.0769 [astro-ph.CO].
- [32] R. A. Battye, B. Garbrecht, and A. Moss, JCAP **0609**, 007 (2006), arXiv:astro-ph/0607339.
- [33] P. Ade *et al.* (Planck Collaboration), (2013), arXiv:1303.5085 [astro-ph.CO].
- [34] P. Ade *et al.* (Planck Collaboration), (2013), arXiv:1303.5084 [astro-ph.CO].
- [35] D. H. Lyth, (2012), arXiv:1201.4312 [astro-ph.CO].
- [36] E. Bugaev and P. Klimai, JCAP **1111**, 028 (2011), arXiv:1107.3754 [astro-ph.CO].
- [37] E. Bugaev and P. Klimai, Phys.Rev. **D85**, 103504 (2012), arXiv:1112.5601 [astro-ph.CO].
- [38] J.-O. Gong and M. Sasaki, (2010), arXiv:1010.3405 [astro-ph.CO].
- [39] J. Fonseca, M. Sasaki, and D. Wands, (2010), arXiv:1005.4053 [astro-ph.CO].
- [40] A. A. Abolhasani and H. Firouzjahi, (2010), arXiv:1005.2934 [hep-th].
- [41] L. Alabidi and D. Lyth, JCAP **0608**, 006 (2006), arXiv:astro-ph/0604569.
- [42] D. H. Lyth, (2010), arXiv:1005.2461 [astro-ph.CO].
- [43] K. Enqvist and A. Vaihkonen, JCAP **0409**, 006 (2004), arXiv:hep-ph/0405103.
- [44] N. Barnaby and J. M. Cline, Phys. Rev. **D75**, 086004 (2007), arXiv:astro-ph/0611750.
- [45] N. Barnaby and J. M. Cline, Phys. Rev. **D73**, 106012 (2006), arXiv:astro-ph/0601481.
- [46] L. Alabidi, JCAP **0610**, 015 (2006), arXiv:astro-ph/0604611.
- [47] D. Mulryne, S. Orani, and A. Rajantie, Phys. Rev. **D84**, 123527 (2011), arXiv:1107.4739 [hep-th].
- [48] A. Avgoustidis, S. Cremonini, A.-C. Davis, R. H. Ribeiro, K. Turzynski, *et al.*, JCAP **1202**, 038 (2012), arXiv:1110.4081 [astro-ph.CO].
- [49] D. Langlois, F. Vernizzi, and D. Wands, JCAP **0812**, 004 (2008), arXiv:0809.4646 [astro-ph].
- [50] C. Gordon, D. Wands, B. A. Bassett, and R. Maartens, Phys. Rev. **D63**, 023506 (2001), arXiv:astro-ph/0009131.
- [51] N. S. Sugiyama, E. Komatsu, and T. Futamase, Phys.Rev. **D87**, 023530 (2013), arXiv:1208.1073 [gr-qc].
- [52] D. H. Lyth and Y. Rodriguez, Phys.Rev.Lett. **95**, 121302 (2005), arXiv:astro-ph/0504045 [astro-ph].
- [53] C. Ringeval, Lect.Notes Phys. **738**, 243 (2008), arXiv:astro-ph/0703486 [ASTRO-PH].
- [54] L. Kofman, A. D. Linde, and A. A. Starobinsky, Phys. Rev. **D56**, 3258 (1997), hep-ph/9704452.
- [55] J. Garcia-Bellido and A. D. Linde, Phys. Rev. **D57**, 6075 (1998), hep-ph/9711360.
- [56] G. N. Felder *et al.*, Phys. Rev. Lett. **87**, 011601 (2001), hep-ph/0012142.
- [57] G. N. Felder, L. Kofman, and A. D. Linde, Phys. Rev. **D64**, 123517 (2001), arXiv:hep-th/0106179.
- [58] E. J. Copeland, S. Pascoli, and A. Rajantie, Phys. Rev. **D65**, 103517 (2002), arXiv:hep-ph/0202031.
- [59] V. N. Senoguz and Q. Shafi, Phys. Rev. **D71**, 043514 (2005), hep-ph/0412102.
- [60] G. Leung, E. R. Tarrant, C. T. Byrnes, and E. J. Copeland, JCAP **1209**, 008 (2012), arXiv:1206.5196 [astro-ph.CO].
- [61] J. Martin and V. Vennin, Phys. Rev. **D85**, 043525 (2012), arXiv:1110.2070 [astro-ph.CO].

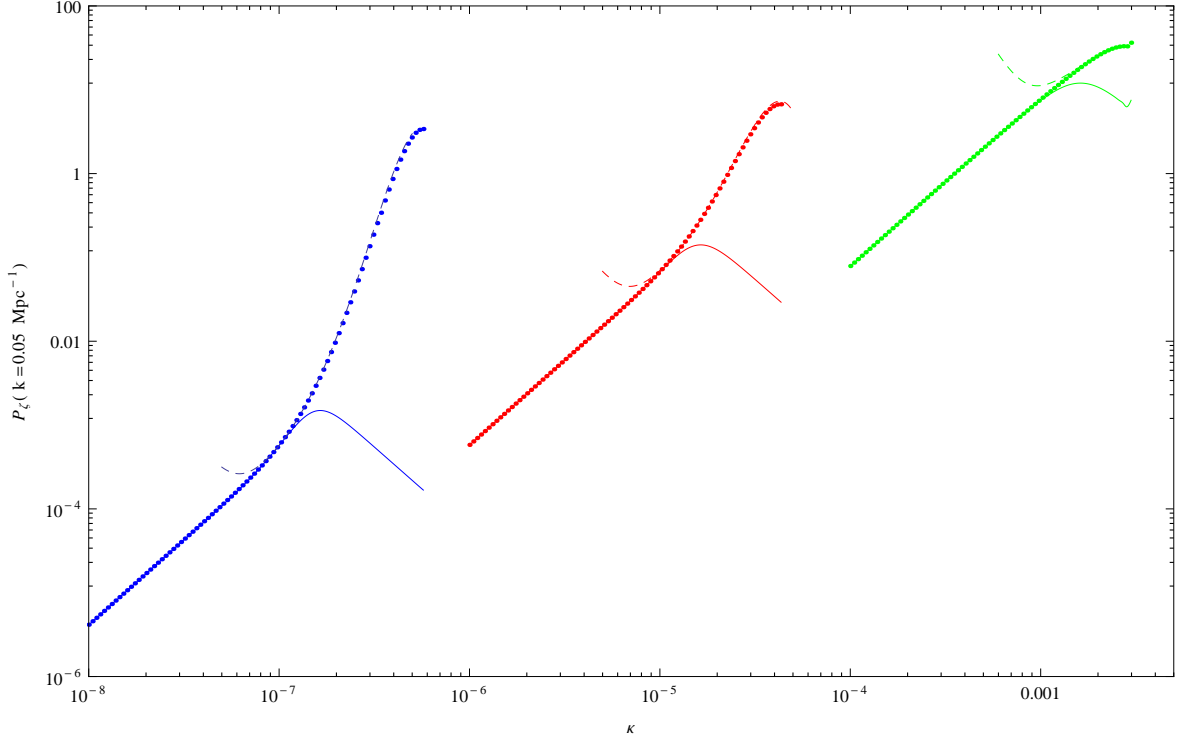


FIG. 4. Amplitude of the power spectrum of curvature perturbations from the analytic approximations based on the δN formalism (Hubble exit in phase 1: dashed), from the numerical integration (points), and assuming effectively single field trajectories (solid) as a function of the κ parameter for the F-term model, for a pivot scale $k_* = 0.05 \text{ Mpc}^{-1}$, and from left to right, $m = 10^{-3}/10^{-2}/10^{-1}$.

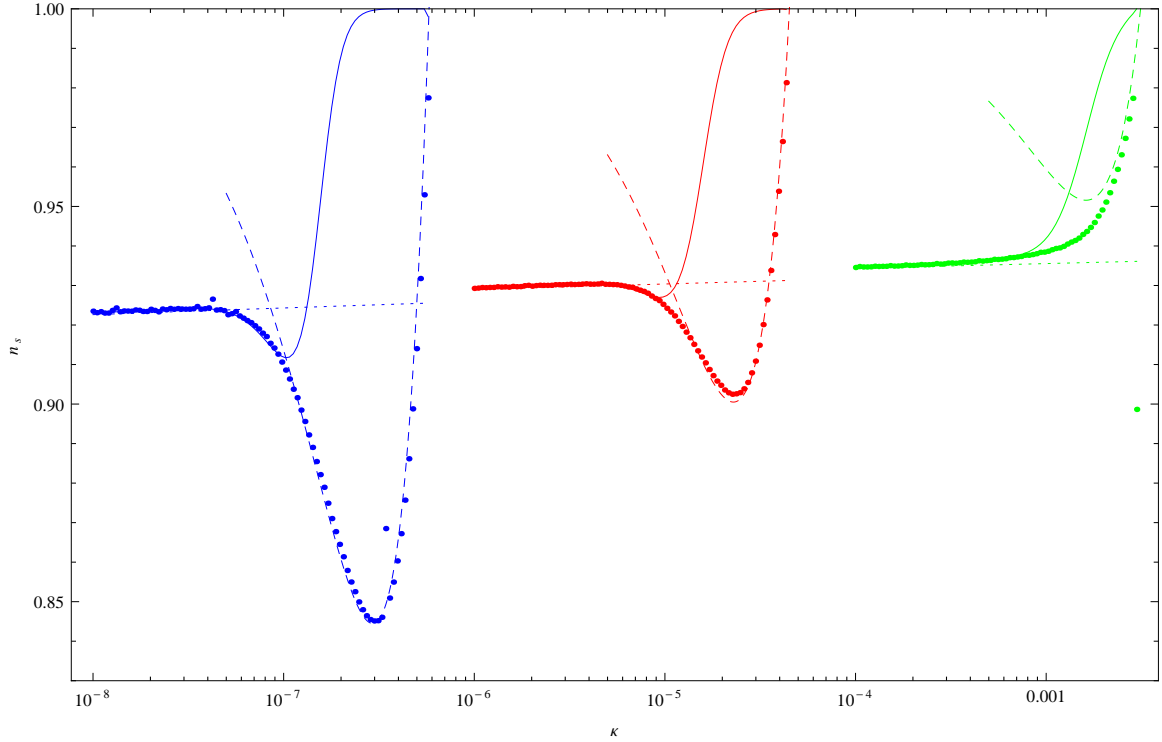


FIG. 5. Spectral index of the power spectrum of curvature perturbations derived from the analytic approximations based on the δN formalism (Hubble exit in phase 1: dashed / phase 2: short dashed), derived from the numerical integration (points), and assuming effectively single field trajectories (solid), as a function of the κ parameter for the F-term model, for a pivot scale $k_* = 0.05 \text{ Mpc}^{-1}$, and from left to right, $m = 10^{-3}/10^{-2}/10^{-1}$.